

REPORT DOCUMENTATION PAGE			Form Approved OMB No. 0704-0188	
Public reporting burden for this collection of information is estimated to average 1 hour per response, including the time for reviewing instructions, searching existing data sources, gathering and maintaining the data needed, and completing and reviewing the collection of information. Send comments regarding this burden estimate or any other aspect of this collection of information, including suggestions for reducing this burden, to Washington Headquarters Services, Directorate for Information Operations and Reports, 1215 Jefferson Davis Highway, Suite 1204, Arlington, VA 22202-4302, and to the Office of Management and Budget, Paperwork Reduction Project (0704-0188), Washington, DC 20503.				
1. AGENCY USE ONLY (Leave blank)	2. REPORT DATE 30.Jun.99	3. REPORT TYPE AND DATES COVERED THESIS		
4. TITLE AND SUBTITLE ANALYSIS OF A NATURAL CONVECTION/THERMOSYPHON MECHANISM FOR HEAT REJECTION FROM ENCLOSURES		5. FUNDING NUMBERS		
6. AUTHOR(S) 2D LT STAHL JAMES W				
7. PERFORMING ORGANIZATION NAME(S) AND ADDRESS(ES) UNIVERSITY OF TEXAS AUSTIN		8. PERFORMING ORGANIZATION REPORT NUMBER		
9. SPONSORING/MONITORING AGENCY NAME(S) AND ADDRESS(ES) THE DEPARTMENT OF THE AIR FORCE AFIT/CIA, BLDG 125 2950 P STREET WPAFB OH 45433		10. SPONSORING/MONITORING AGENCY REPORT NUMBER FY99-150		
11. SUPPLEMENTARY NOTES				
12a. DISTRIBUTION AVAILABILITY STATEMENT Unlimited distribution In Accordance With AFI 35-205/AFIT Sup 1		12b. DISTRIBUTION CODE		
13. ABSTRACT (Maximum 200 words)				
<p style="font-size: 2em; margin: 0;">19990805 085</p> <p style="font-size: 1.5em; margin: 10px 0;">DISTRIBUTION STATEMENT A Approved for Public Release Distribution Unlimited</p>				
14. SUBJECT TERMS		15. NUMBER OF PAGES 87		
		16. PRICE CODE		
17. SECURITY CLASSIFICATION OF REPORT	18. SECURITY CLASSIFICATION OF THIS PAGE	19. SECURITY CLASSIFICATION OF ABSTRACT	20. LIMITATION OF ABSTRACT	

Analysis of a Natural Convection/Thermosyphon
Mechanism for Heat Rejection from Enclosures

by

James Wilson Stahl, B.S.

Thesis

Presented to the Faculty of the Graduate School
of the University of Texas at Austin
in Partial Fulfillment
of the Requirements
for the Degree of

Master of Science in Engineering

The University of Texas at Austin
August 1998

Analysis of a Natural Convection/Thermosyphon
Mechanism for Heat Rejection from Enclosures

APPROVED BY

SUPERVISING COMMITTEE:

Gary C. Vleet
of the G. J.

To my parents John and Lana

ACKNOWLEDGMENTS

The author would like to thank Dr. Gary C. Vliet for advisement, and guidance in the completion of this thesis. It would have been an impossibility without his time, patience, and expertise. He was instrumental in helping the author achieve the goal of obtaining a master's degree in one year.

J.W.S.

The University of Texas at Austin

August 13, 1998

Analysis of a Natural Convection/Thermosyphon
Mechanism for Heat Rejection from Enclosures

by

James Wilson Stahl, M.S.E.

The University of Texas at Austin

SUPERVISOR: Gary C. Vliet

The problem of electronic component cooling in rectangular tall vertical enclosures heated at the bottom, and cooled from the sides and top is investigated numerically. The investigation considers both 2-D and 3-D enclosures, with emphasis on the 2-D configuration. Several performance parameters are considered. The maximum power that can be dissipated from these enclosures is found for varying aspect ratios, with consideration given to radiation effects, finning, and heater geometry. Limiting criteria are that the air temperature below the heated elements be 343 K with a 298 K ambient. Heat rejection for all configurations was almost linear with aspect ratio (enclosure area). The plane wall with radiation exhibited significantly better cooling at higher aspect ratios while the optimally finned wall exhibited improved cooling at lower aspect ratios. The effects of radiation and finning are nearly additive when combined. The results comparing the 2-D and 3-D plane wall enclosures showed very close agreement and heater element configuration was shown to have small effects on cooling performance.

TABLE OF CONTENTS

	<u>Page</u>
Chapter 1: General Information.....	1
1.1 Introduction	1
1.2 Literature Review	3
1.3 Objective	6
Chapter 2: Problem Definition	8
2.1 Geometry.....	8
2.2 Fluent.....	12
2.3 Boundary Conditions.....	13
2.4 Performance Qualifier.....	14
Chapter 3: Assumptions and Mathematical Technique.....	16
3.1 Laminar Flow Assumptions.....	16
3.2 Neglect of Viscous Dissipation.....	16
3.3 Bousinessq Approximation.....	17
3.4 Fluid Properties	17
3.5 Enclosure Walls.....	18
3.6 External Heat Transfer Coefficient for Plane Walls.....	19
3.7 External Heat Transfer Coefficient for Finned Surfaces.....	21
3.8 Inclusion of Radiation.....	24
Chapter 4: Numerical Results.....	27
4.1 2-D Plane Wall Analysis without Radiation.....	27
4.2 2-D Smooth Wall with Radiation.....	30

4.3 2-D Finned Wall Analysis.....	32
4.4 2-D Finned Wall with Radiation.....	39
4.5 3-D Plane Wall without Radiation.....	41
4.6 2-D Heater Element Size Effects.....	43
Chapter 5: Comparisons and Discussion.....	44
5.1 2-D Comparisons.....	44
5.2 2-D and 3-D Comparison.....	48
5.3 FLUENT Temperature and Contour Plots.....	50
Chapter 6: Conclusion and Recommendations.....	52
6.1 Conclusion.....	52
6.2 Recommendations.....	53
Appendix A: 2-D Plane Wall Temperature Contour Plots.....	55
A.1 $AR = 1$	56
A.2 $AR = 2$	57
A.3 $AR = 3$	58
A.4 $AR = 4$	59
A.5 $AR = 6$	60
A.6 $AR = 8$	61
A.7 $AR = 10$	62
Appendix B: 2-D Plane Wall Velocity Contour Plots.....	63
B.1 $AR = 1$	64
B.2 $AR = 2$	65
B.3 $AR = 3$	66

B.4 AR= 4.....	67
B.5 AR = 6.....	68
B.6 AR = 8.....	69
B.7 AR = 10.....	70
Appendix C: Temperature Contour Plots for AR =2.....	71
C.1 No Fins, Radiation	72
C.2 Fins, No Radiation (Near Fin).....	73
C.3 Fins, No Radiation (Between Fins).....	74
C.4 Fins & Radiation (Near Fin).....	75
C.5 Fins & Radiation (Between Fins).....	76
C.6 3-D Plane Wall (At Centerline).....	77
Appendix D: Velocity Contour Plots for AR =2.....	78
D.1 No Fins, Radiation.....	79
D.2 Fins, No Radiation (Near Fin).....	80
D.3 Fins, No Radiation (Between Fins).....	81
D.4 Fins & Radiation (Near Fin).....	82
D.5 Fins & Radiation (Between Fins).....	83
D.6 3-D Plane Wall (At Centerline).....	84
Bibliography.....	85
Vita.....	87

LIST OF TABLES

<u>Table</u>	<u>Page</u>
4.1: Effect of Aspect Ratio on Q_{\max} and Key Temperatures (2-D No Fins or Radiation)	28
4.2: Effect of Aspect Ratio on Q_{\max} and Key Temperatures (2-D, With Radiation, No Fins)	31
4.3: Effect of Fin Geometry on Q_{\max} for $AR=2$ (2-D, No Radiation)	33
4.4: Effect of Aspect Ratio on Q_{opt} and Key Temperatures (2-D, Fins, No Radiation).....	37
4.5: Effect of Aspect Ratio on Q_{opt} and Key Temperatures (2-D, Fins and Radiation).....	39
4.6: Effect of Aspect Ratio on Q_{\max} and Key Temperatures (3-D, No Fins or Radiation).....	41
4.7: Q_{\max} Vs. Heater Element Thickness.....	43
5.1: Comparison of Q_{\max} values for 2-D Cases.....	44
5.2: Comparison of the Heat Rejection per Unit Area of Enclosure for 2-D and 3-D Cases.....	49

LIST OF FIGURES

<u>Figure</u>	<u>Page</u>
2.1: Problem Geometry.....	9
2.2: Symmetry Lines for 2-D Fin Cases.....	11
4.1: Q_{max} Vs. Aspect Ratio (2-D, No Fins or Radiation).....	28
4.2: Key Temperatures Vs. Aspect Ratio (2-D, No Fins or Radiation)...	29
4.3: Q_{max} Vs. Aspect Ratio (2-D, With Radiation, No Fins).....	31
4.4: Key Temperatures Vs. Aspect Ratio (2-D, With Radiation, No Fins).....	32
4.5: Heat Rejection as a Function of Fin Height for a Constant Height to Spacing Quotient and $AR=2$	34
4.6: Boundary Layer Comparison for Configurations Having Comparable Fin Volume but Different Height and Spacing.....	36
4.7: Q_{opt} Vs. Aspect Ratio (2-D, Fins, No Radiation).....	38
4.8: Key Temperatures Vs. Aspect Ratio (2-D, Fins, No Radiation).....	38
4.9: Q_{opt} Vs. Aspect Ratio (2-D Fins and Radiation).....	40
4.10: Key Temperatures Vs. Aspect Ratio (2-D, Fins and Radiation).....	40
4.11: Q_{max} Vs. Aspect Ratio (3-D, No Fins or Radiation).....	42
4.12: Key Temperatures Vs. Aspect Ratio (3-D, No Fins or Radiation).....	42
5.1: Comparison of Power Dissipation with Aspect Ratio for Various 2-D Cases.....	46

5.2: Enclosure Surface Temperatures Vs. Aspect Ratio.....	46
5.3: Maximum Temperatures Vs. Aspect Ratio.....	47
5.4: Plume Temperatures Vs. Aspect Ratio.....	48
5.5: Velocity Profile Above Heaters (0.25L).....	51

LIST OF SYMBOLS

A_b = unfinned area (m^2)

AR = aspect ratio

A_s = surface area of the enclosure (m^2)

A_t = total surface area of the enclosure (m^2)

b_f = distance between fins (m)

Br = Brinkman number

D = arbitrary 2-D cavity depth (m)

g = acceleration of gravity (m/s^2)

Gr_L = Grashof number based on length

h_e = vertical height of each heated element (m)

h_{eff} = effective external heat transfer coefficient for finned cases (W/m^2 K)

h_f = height of each fin (m)

\bar{h} = average external heat transfer coefficient (W/m^2 K)

\bar{h}_{2d} = average external heat transfer coefficient for 2-D cases (W/m^2 K)

k = thermal conductivity of air (W/m K)

k_f = thermal conductivity of the fins (W/m K)

L = cavity height (m)

n = number of heated elements

Nu_{cond} = Nusslet number for conduction limiting

Pr = Prandtl number

Q_{max} = power dissipated in heater elements (W/m for 2-D, W for 3-D)

Q_{opt} = power dissipated for optimum fin configuration (W/m)

q'''_{gen} = volumetric heat generation rate from heated elements (W/m^3)

Ra_L = Rayleigh number based on length

Ra_n = nominal Rayleigh number

t_e = thickness of each element (m)

t_f = thickness of each fin (m)

T_b = temperature at the bottom of the enclosure (K)

T_m = maximum temperature (K)

T_p = plume temperature (K)

T_s = average temperature of enclosure surface (K)

T_∞ = ambient air temperature (K)

V = velocity (m/s^2)

V_e = total volume of heated elements (m^3)

W = cavity width (m)

α = thermal diffusivity of air (m^2/s)

β = coefficient of thermal expansion of air ($1/K$)

ΔT = average temperature difference (K)

ΔT_n = nominal temperature difference (K)

ε = emissivity

ν = kinematic viscosity of air (m^2/s)

μ = dynamic viscosity of air ($kg/m\ s$)

ρ = density of air (kg/m^3)

ρ_o = reference density of air (kg/m^3)

CHAPTER 1: GENERAL INFORMATION

1.1 Introduction

The study of heat transfer in convection flows inside rectangular enclosures driven by the buoyancy force has been stimulated recently by applications related to electronic equipment cooling. The cooling of electronic systems receives ever increasing attention by the scientific and technical community, as is apparent by the exponential increase in the number of papers devoted to the subject. Cooling of electronics systems (i.e. cabinets, computers, and telecommunications equipment) is one of the major problems in electronics as the industry strives for miniaturization, lower noise levels, and the increasing demands for more reliable products. Furthermore, tremendous advancements in chip technology focusing on the ability to increase the number of electronic circuits per chip has highlighted the importance of the thermal control problem. The energy generated in these electronic components must be effectively carried away in order to maintain their temperatures below the maximum operating limit, otherwise the electronic system may not function properly or the operational life could be shortened.

A variety of different cooling techniques maintain the operating temperature of chip devices within safe functional levels. Whenever it

can be used, natural convection is still the preferred technique for cooling electronic components. Besides being relatively simple, natural convection techniques are inexpensive, safe, quiet, and maintenance free (Johnson 1986).

The concern over cooling of electronic equipment ranges from heat transfer from an active element to the encapsulation, heat transfer from individual chips to the coolant, to heat transfer from one or more circuit boards to the ambient. The current study is directed at the latter. One concept for heat rejection is to enclose the heat dissipating components in a vertical cavity with the elements near the bottom. The dissipated heat is transported by a thermosyphon flow from the heated elements to the walls above, and then by natural convection from the walls on the exterior to ambient air. Conceptually, fans could be incorporated to enhance flow, but such a configuration is not considered here. The term thermosyphoning refers to circulation within an enclosure when there is a lower heated region and upper cooler surface. Thermosyphoning occurs naturally due to a buoyant driving force caused by the density variation around the loop. Closed loop thermosyphoning is a reliable method of thermal energy transfer from a heat source to a heat sink at a higher level. The combined natural convection/thermosyphon mechanism is the focus of this study.

1.2 Literature Review

Despite the growing importance of electronic component cooling, most studies continue to restrict their consideration almost exclusively to the case of two-dimensional rectangular enclosures with vertical isothermal walls at different temperatures. Relatively little work has been carried out on more complex boundary conditions, and the three-dimensional case has not been analyzed extensively, except for specific geometries of interest. Furthermore, little consideration has been given to many of the factors affecting the amount of cooling taking place. Performance factors that should be considered include material selection, enclosure aspect ratio, heated element location and size, radiation effects, and finning. Very few have studied the effects of cavity width or aspect ratio (i.e. channel height to width ratio) on the heat transfer characteristics of discretely heated channels or enclosures.

The study of Chu et al. (1976) appears to be one of the first published investigations dealing with natural convection in an enclosure with localized heating. The case considered an isothermal heated strip located in one of the cavity's vertical walls with the opposing wall uniformly cooled. Important results regarding this study included the effects of heater size, location, enclosure aspect ratio, and the influence of top and bottom wall boundary conditions. Increasing the cavity aspect ratio generally promoted heat transfer for isothermal horizontal walls, but reduced it for the adiabatic horizontal surfaces.

Shen et al. (1989) numerically studied the effect of aspect ratio on natural convection in a discretely heated vertical wall with the other wall considered as a heat sink. The effect of aspect ratio on the local and overall heat transfer rates was determined to be relatively minor. This study was later followed up by Prasad et al. (1990), who found the effect of aspect ratio on maximum temperature to be minimal for aspect ratio's greater than 3.0.

Ganzarolli and Milanez (1994) recently studied a rectangular tall cavity heated from below and symmetrically cooled from the sides with the top wall being insulated. Aspect ratio's (height/width) for this cavity were varied between 1 and 9. The study was performed to observe the influence of aspect ratio on the heat transfer and flow field. By performing numerical simulations, they showed that for certain cases, heating of the cavity floor does not affect the cavity upper region, resulting in what Poulikakos (1985) called "incomplete thermal penetration." Numerical results were obtained for air ($Pr=0.7$) and for values of Rayleigh number between 10^3 and 10^7 . It was observed that as the aspect ratio was increased, the streamlines and the isotherms tend to concentrate near the cavity floor, while the fluid in the upper region remains practically stationary and isothermal. This effect is called "incomplete thermal penetration" because the upper region is comparatively less affected by the heated floor. The increase in aspect ratio tends to accentuate this effect.

Additionally, Ganzarolli and Milanez held the aspect ratio constant and varied the Rayleigh number. It was found that higher Rayleigh numbers had more influence on the flow field along the cavity height. The center of the streamlines is dislocated upwards and the flow, at higher Rayleigh numbers, tends to occupy the whole cavity. They also noted that the isotherms tended to be compressed near the heated cavity floor. Ultimately, they showed that higher values of aspect ratio ($AR > 3$), and moderate values of the Rayleigh number ($Ra \leq 10^6$) produce natural convection flows which can result in incomplete thermal penetration, with the cavity region remaining almost isothermal.

Presently, the state of the art in thermal management of electronic systems is reported by Bar-Cohen (1992) and more recently with several of their newer papers. However, their designs are always restricted to highly specific problems. They have yet to fully explore the general design information and trends associated with natural convection cooling of electronic components.

The studies above have examined the characteristics of thermosyphon flows in enclosures where the heat dissipating surfaces are either the cavity floor, or a portion of one wall. The geometry considered in this work assumes the generation to occur in a 'porous region' near the cavity bottom with natural convection occurring on the exterior of the vertical cavity walls.

1.3 Objective

The work reported here attempts to extend the analysis to the case where a stack may be located above a heated enclosure. In accomplishing this, it would seem that a sensitivity comparison would be beneficial in aiding in the design of enclosures for electronic component cooling. Given the cabinet dimensions, the number of printed circuit boards, and the power to be dissipated, the designer must deal with a large number of parameters which influence the local velocity fields and as a consequence the local component temperatures. Some pertinent design parameters include enclosure geometry (width and aspect ratio), radiation effects, finning, material selection, heated element location, heated element size, and heat generation.

Specifically, an analysis of a natural convection/thermosyphon mechanism for heat rejection from a tall rectangular enclosure heated from below and symmetrically cooled from the sides and top is analyzed. This study is intended to observe the influence of the aspect ratio among other design parameters on the heat transfer and flow field. On the exterior of the enclosure, natural convection becomes the mechanism for heat rejection. On the interior of the enclosure, a thermosyphon, characterized by density variation, enables a buoyancy induced flow circulation that continually cools the heated elements contained within the enclosure. The interior fluid (air) is hermetically isolated from the outside ambient air. FLUENT is used to determine the

steady state solution to this natural convection problem by using the Boussinesq approximation for density variation. Two-dimensional numerical simulations are performed for the combined convection-conduction problem. A three-dimensional case is also examined so as to compare with the results of the two dimensional cases.

Other design aspects that are analyzed include external radiation effects, the optimization of fin size and spacing, and heated element geometry. By examining the relative effects of aspect ratio, radiation, finning, and heater element geometry, an optimal enclosure configuration for a desired amount of heat rejection may be determined.

CHAPTER 2: PROBLEM DEFINITION

2.1 Geometry

The geometry considered consists of a cavity with the heat dissipation originating from a 'porous region' near the bottom that could simulate electronic circuit boards. Thermosyphon flow between this region and the cooler cavity walls above is driven by buoyant forces. Natural convection on the exterior walls transfers the dissipated heat to the ambient. In practice this would be a three-dimensional cavity, but as noted the study emphasizes the two-dimensional geometry, the results of which are compared to limited simulations for the three-dimensional geometry. In addition, the cavity walls may be plane or finned, and radiation may be an important mechanism. The geometry used to represent the enclosure investigated in this study can be seen in Figure 2.1. A rectangular geometry with a square cross-section was chosen. In reality, a cylindrical geometry may be just as effective at dissipating heat, and may be cheaper to produce. However, the increased difficulty in modeling and solving of a cylindrical geometry by FLUENT led to the choice of a Cartesian system. In order to reduce the number of parameters for optimization, the enclosure cross-section is selected to be 10 cm by 10 cm for the three-dimensional

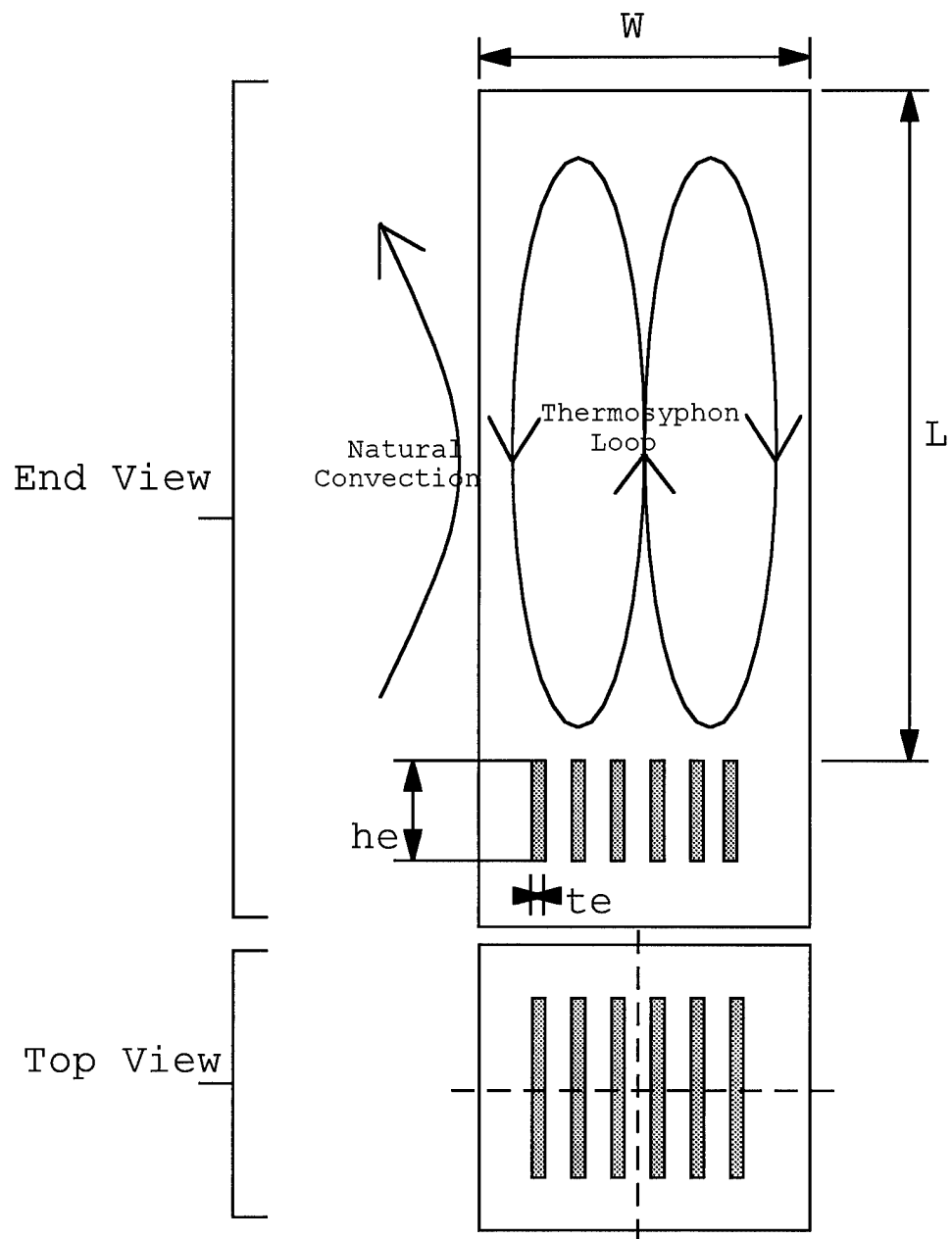


Figure 2.1: Problem Geometry

case. The height of the enclosure above the heated region is varied from 10 cm to 100 cm ($AR=1$ to 10).

Located near the bottom of the enclosure is a region containing several heat dissipating elements. This region has the same square cross-section as the enclosure, 10 cm X 10 cm, is 5 cm high, and is assumed to be perfectly insulated. Six heated elements are specified, each 0.4 cm thick, 3 cm high, 6 cm long, and spaced at one centimeter on centers. This represents a heated region with about 2 cm clearance between the walls of the enclosure bottom.

For the two-dimensional geometry the heated elements are assumed to be very long, and would appear as the upper portion of Figure 2.1 when viewed from the end. The dimensions for the heated elements were chosen to be somewhat representative of printed circuit boards.

When analyzing a two-dimensional case with fins, a three-dimensional geometry must be employed as shown in Figure 2.2. The height and width of the enclosure remains the same, and the fin spacing becomes the third dimension. Taking into account the planes of symmetry, the region to be analyzed is the shaded area of Figure 2.2. Note that half of this region could have been used if desired.

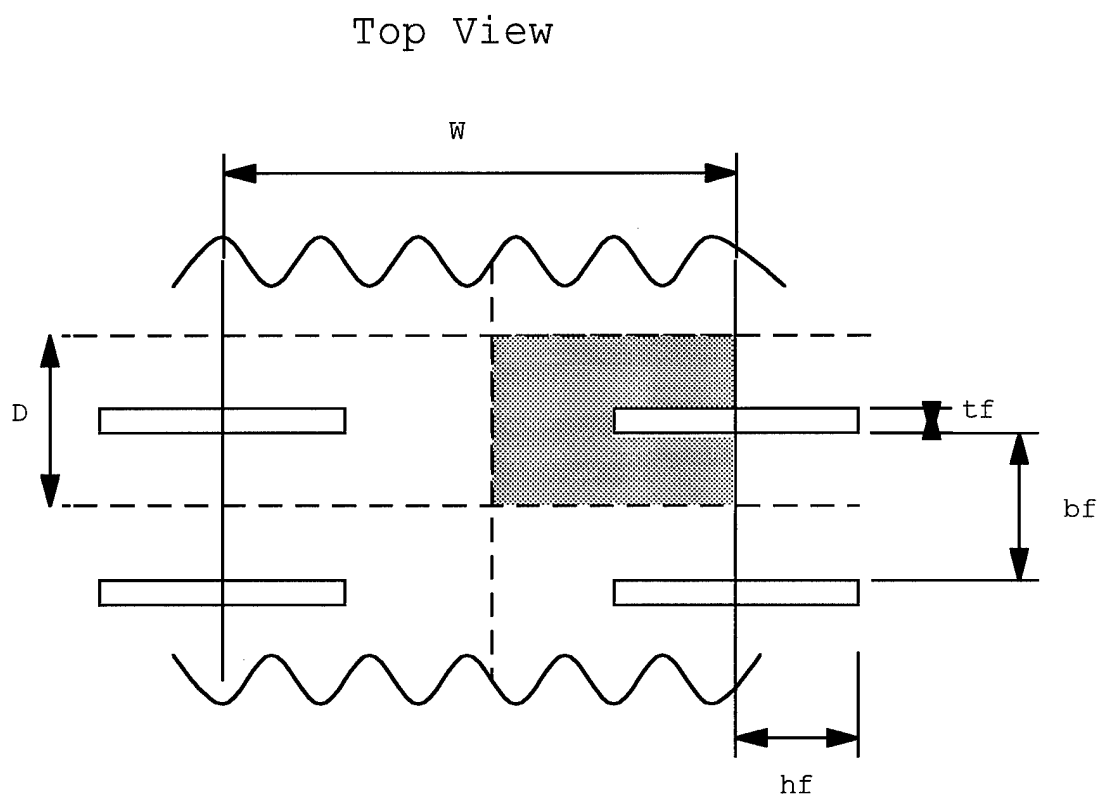


Figure 2.2 : Symmetry Lines for 2-D Fin Cases

2.2 FLUENT

There are several codes capable of modeling convection flows; FLUENT was chosen for this investigation. This code models the flow and heat transfer by solving the conservation equations for mass, momentum, and energy. The governing equations are discretized on a curvilinear grid to enable computations in complex geometries. A non-staggered system is used for storage of discrete velocities, temperatures, and pressures. Interpolation is accomplished via a first-order power law scheme. The equations are solved using SIMPLE-like algorithms with an iterative line by line matrix solver and multigrid acceleration.

To ensure that the resulting outputs were accurate, a determination of the necessary grid spacing was performed. FLUENT's primary requirement for grid spacing is the number of computational cells located near walls. This is due to the aggressive gradients that are many times located in these regions. Specifically, parallel plates separated by a height of H , should adhere to the requirements stated in Equation 2.1.

$$\frac{\Delta n}{H} \leq .05 \quad (2.1)$$

For the problems conducted in this simulation this value came out to be 0.01 or 0.02, depending on the specific case. This value is less than the maximum value of 0.05. Additionally, FLUENT requires that no flow

passage be less than three cells wide. Finally, the last criteria requires that each individual cell have an aspect ratio of less than ten. All these criteria were met. To further ensure accuracy, test cases were run to find the optimal grid spacing.

2.3 Boundary Conditions

There are three boundary conditions that must be specified in order for the problem to be solved by FLUENT. The first boundary condition is one of non-slip adiabatic surfaces for the floor of the enclosure and walls adjacent to the heated elements. This assumes heat is lost only from the enclosure walls above the heated elements. The enclosure surfaces above the heated region are also assumed to be non-slip, and on the exterior surfaces convection or convection and radiation is prescribed. The user must define an external heat transfer coefficient, and an external ambient air temperature. To include radiation, the user must additionally define the emissivity of the external surface of the enclosure, as well as the external radiation sink temperature. The third type of boundary is the surface of the heated elements. The heated elements are treated as generating and conducting material with the wall thermal conductivity, and a volumetric heat generation rate prescribed. At the surfaces of these elements, solid conduction to the surface is balanced by convection to the gas and there is a no-slip

condition for the gas. For the upper enclosure walls it was assumed that the wall transverse resistance was negligible, but that the longitudinal resistance was infinite.

When fins were included, an effective heat transfer coefficient for the exterior finned surfaces was computed from correlations and input into FLUENT. For the interior fins, the fin material thermal conductivity was specified and the convection/conduction interaction was solved by FLUENT. In all fin cases a thermal conductivity representative of aluminum is used ($k_f=200$).

Only one case of radiation was considered, that of perfectly black exterior surfaces ($\epsilon=1$). Thus, whether the exterior surfaces were plane or finned, the radiation was actually that from a plane surface at the enclosure wall temperature, since the fin efficiencies are near one.

2.4 Performance Qualifier

For all cases the driving factor in performance centered around securing the appropriate mean temperature of the fluid approaching the heated region from below. The mean approach temperature is defined as the temperature near the bottom of the cavity below the heated elements. David Hall (IBM) suggested an approach temperature of approximately 70°C or 343 K for circuit board cooling. Thus, performance of each enclosure is limited by this requirement, and an

assumed 298 K ambient. The goal is to maximize the amount of heat that can be dissipated from the enclosure, while maintaining the average approach temperature of 343 K.

CHAPTER 3: ASSUMPTIONS AND MATHEMATICAL TECHNIQUES

3.1 Laminar Flow Assumption

The problem presented here is assumed to take place in the laminar flow regime. This is a common assumption for many natural convection problems, due to the relatively small velocities (usually not much more than 2 m/s, Mills 1995), and small to modest length scales. Since there is no obvious characteristic velocity for natural convection flows, the Grashof and Rayleigh numbers replace the Reynolds number as the important parameters used to characterize buoyancy induced flows. For the geometries presented here the Rayleigh number based on length falls between about 26 and 26,000 which is well below the critical value of 10^9 for transition to turbulence for vertical walls (Mills 1995). Equation 3.1 defines the Rayleigh number.

$$Ra_L = Gr_L Pr = \frac{g\beta\Delta TL^3}{\nu^2} Pr \quad (3.1)$$

3.2 Neglect Of Viscous Dissipation

Viscous dissipation can be neglected for this problem. The fluid velocities associated with natural convection, and the relatively low viscosity of air ensure that this is a safe assumption. The Brinkman

number is defined in Equation 3.2, and turns out to be much less than the critical value of 1.

$$Br = \frac{V^2 \mu}{k \Delta T} \quad (3.2)$$

3.3 Bousinessq Approximation

Air is assumed to be the working fluid both within the enclosure and external to the enclosure. The Bousinessq approximation is used to model the buoyancy force encountered in this problem. FLUENT calculates the density by defining a reference density, and using the coefficient of thermal expansion and temperature difference. Equation 3.3 shows the method by which FLUENT employs this approximation.

$$\begin{aligned} (\rho - \rho_o)g &= -\rho_o \beta (T - T_o)g \\ \rho &= \rho_o (1 - \beta \Delta T) \end{aligned} \quad (3.3)$$

3.4 Fluid Properties

The material properties for air for this problem were defined as linear functions of temperature in most cases. The linear interpolation was calculated using a temperature range from 300 K to 400 K. The properties that used this approximation were thermal conductivity,

constant pressure specific heat capacity, and molecular viscosity. Other values such as the reference density, buoyancy reference temperature (used in specifying the coefficient of thermal expansion), enthalpy reference temperature, external ambient temperature, heated element thermal conductivity, and fin thermal conductivity were assumed to be constant. Inputs such as the volumetric heat generation rate and external heat transfer coefficient were specified for each case.

3.5 Enclosure Walls

In all cases the walls were assumed to be macroscopically smooth. Furthermore, it was assumed that there was negligible wall conduction longitudinally, and negligible resistance transversely. Reasoning behind this assumption derived from the fact that enclosure thicknesses would be very small. For a wall thickness of 2 mm, the conductance would be approximately $10^5 \text{ W/m}^2\text{-K}$ for aluminum and about $300 \text{ W/m}^2\text{-K}$ for a plastic, while typical natural convection heat transfer coefficients are on the order of 10. Thus, wall transverse resistance can be neglected. However, since the length to thickness of the walls would be of the order of 100, the longitudinal resistance will be large. Therefore, for the purpose of this simulation all enclosure walls are assumed to have negligible transverse resistance and infinite longitudinal resistance. To ensure the validity of the assumption,

several test cases were conducted and all showed that wall conduction had an insignificant effect on cooling performance.

3.6 External Heat Transfer Coefficient for Plane Walls

One approach would have been for FLUENT to simulate the combined interior and exterior flow fields. However, this would have necessitated a much larger grid and resulted in much greater computational time. Fortunately, there are reasonably good correlations for natural convection on surfaces, either plane or finned. Thus, the interior flow field was simulated by FLUENT, and correlations for the external natural convection coefficients were prescribed.

A correlation (Eq 3.4) for the average heat transfer coefficient on vertical plane surfaces in laminar natural convection with constant q'' is proposed by Vliet (1969).

$$\bar{h} = 0.60k \left[\frac{g\beta \text{Pr}}{kv^2} \right]^{1/5} \left(\frac{q''}{L} \right)^{1/5} \quad (3.4)$$

Assuming a mean temperature of 310 K for property evaluation, this equation simplifies to:

$$\bar{h} = 1.26 \left(\frac{q''}{L} \right)^{1/5} \quad (3.5)$$

Knowing that

$$q'' = \frac{\dot{Q}_{gen}}{A_t} = \frac{q'''_{gen} \cdot V_e}{4WL + W^2} \quad (3.6)$$

for a three-dimensional square enclosure of side W , and height L , the average external heat transfer coefficient becomes:

$$\bar{h} = 1.26 \left[\frac{q'''_{gen} \cdot V_e}{W^3 (4AR + 1) AR} \right]^{1/5} \quad (3.7)$$

where AR is the aspect ratio (L/W), q'''_{gen} is the volumetric heat generation in the heated elements, and V_e is the total volume of the heated elements. This correlation allows determination of the appropriate external heat transfer coefficient to be input into FLUENT for the three-dimensional enclosure consisting of plane walls and a flat top. Each time the aspect ratio, or volumetric heat generation rate is changed, a new coefficient must be calculated.

For the two-dimensional case the expression for the average external heat transfer coefficient must be modified. The enclosure now has a cavity width of 10 cm, a height L , and an arbitrary depth, D . The surface area is calculated as:

$$A_t = 2D \cdot L + D \cdot W = D(2L + W) \quad (3.8)$$

and the total volume of the heated elements is:

$$V_e = n \cdot t_e \cdot h_e \cdot D \quad (3.9)$$

For this study there are six elements and each is 0.4 cm by 3 cm in cross section. Substituting the enclosure surface area and heated element volume expressions into Equation 3.6 yields Equation 3.10 for the average heat transfer coefficient for the two-dimensional case. Notice that the arbitrary depth, D , cancels out.

$$\bar{h}_{2D} = 1.26 \left[\frac{q'''_{gen} V_e}{W^2 (2AR + 1) AR} \right]^{1/5} \quad (3.10)$$

3.7 External Heat Transfer Coefficient for Finned Surfaces

In this numerical simulation, FLUENT uses a prescribed heat transfer coefficient on the exterior surface, which for FLUENT is assumed to be a plane surface. Thus, in the case of finned external surfaces, an effective external heat transfer coefficient based on a hypothetical plane surface must be evaluated. The effective external heat transfer coefficient for a finned external surface is derived from the correlation proposed by Karagiozis et al. (1994). Their study focused on

natural convection heat transfer from arrays of isothermal fins (assumes 100% fin efficiency). For example this would be a good approximation for aluminum fins of height 3 cm, and 0.3 cm thickness whose efficiency for this application would be about 97%. However, for plastic fins of this dimension the efficiency would be of the order of 30%. The proposed correlation for the Nusselt number for vertical fin orientation over the range for $0.4 < Ra < 4000$ is:

$$Nu - Nu_{COND} = 0.515Ra^{1/4} \left[1 + \left(\frac{3.26}{Ra^{0.21}} \right)^3 \right]^{-1/3} \quad (3.11)$$

where the Rayleigh number and Nusselt number are based on a length scale of b_f and Nu_{COND} is the conduction limiting value, and is provided by Karagiozis for selected fin geometries. Based on Equation 3.11, the expression for the average external heat transfer coefficient becomes:

$$\bar{h} = \frac{k}{b_f} \left\{ 0.515Ra^{1/4} \left[1 + \left(\frac{3.26}{Ra^{0.21}} \right)^3 \right]^{-1/3} + Nu_{cond} \right\} \quad (3.12)$$

While this equation provides an average heat transfer coefficient for the total outside surface area, it must be transformed into the effective heat transfer coefficient, h_{eff} based on the 'plane' exterior surface (at the base

of the fins). On the outside of the enclosure, the heat transfer rate is equal to:

$$Q = \bar{h}A_t(T_s - T_\infty) = h_{eff}A_b(T_s - T_\infty) \quad (3.13)$$

where the total heat transfer area is:

$$A_t = (t_f + 2h_f + b_f)L \quad (3.14)$$

and the effective base area is:

$$A_b = (b_f + t_f)L \quad (3.15)$$

The effective heat transfer coefficient on the outside of the enclosure is thus related to the finned surface heat transfer coefficient by:

$$h_{eff} = \bar{h} \left(\frac{t_f + b_f + 2h_f}{t_f + b_f} \right) \quad (3.16)$$

Combining Equation 3.12 and Equation 3.16, the effective external heat transfer coefficient for the finned surface becomes:

$$h_{eff} = \frac{k}{b_f} \left(\frac{t_f + b_f + 2h_f}{t_f + b_f} \right) \left\{ 0.515 Ra^{1/4} \left[1 + \left(\frac{3.26}{Ra^{0.21}} \right)^3 \right]^{-1/3} + Nu_{cond} \right\} \quad (3.17)$$

Since this correlation includes the Rayleigh number, which is a function of ΔT , rather than the q'' dependence in the correlation for plane vertical surfaces (Eq 3.4), the solution was iterative. FLUENT was run with an h_{eff} based on a nominal Rayleigh number (Ra_n) evaluated at $\Delta T_n = T_{sn} - T_{\infty} = 20^\circ\text{C}$. The effective external heat transfer coefficient was recalculated as new values for the surface temperature of the enclosure, T_s , were found. Iteration was performed until T_s stabilized. Equation 3.18 shows the expression used for this iterative procedure.

$$h_{eff} = \frac{k}{b_f} \left(\frac{t_f + b_f + 2h_f}{t_f + b_f} \right) \left\{ 0.515 Ra_n^{1/4} \left(\frac{\Delta T}{\Delta T_n} \right)^{1/4} \left[1 + \frac{3.26}{Ra_n^{0.21} \left(\frac{\Delta T}{\Delta T_n} \right)^{0.21}} \right]^3 \right]^{-1/3} + Nu_{cond} \right\} \quad (3.18)$$

3.8 Inclusion of Radiation

Some cases involving radiation with perfectly black surfaces were considered. These were iterative in that the external heat transfer

coefficient is a function of ΔT . Values of h (plane wall) or h_{eff} (fins) were calculated, FLUENT was run, and then these values were adjusted. FLUENT was rerun until acceptable convergence was achieved.

For the plane wall including radiation, the following equation was used to calculate the external heat transfer coefficient.

$$\bar{h}_{2D} = 1.26 \left[\frac{q'''_{gen} \cdot n \cdot t_e \cdot h_e}{W^2 (2AR + 1) AR} - \frac{\sigma(T_s^4 - T_\infty^4)}{W \cdot AR} \right]^{1/5} \quad (3.19)$$

The volumetric heat generation rate was guessed, and the value for the surface temperature was found. This value was plugged back into Equation 3.19, and a new enclosure surface temperature was recorded. This procedure continued until T_s stabilized. The volumetric heat generation rate was also adjusted until the desired mean approach temperature of 343 K was achieved. Adjusting both the volumetric heat generation rate and the surface temperature, to achieve 343K at the bottom of the enclosure, proved to be a tedious process.

For the case involving fins with radiation, Equation 3.18 was applied. There were no modifications for this equation because the Rayleigh number is based on $T_s - T_\infty$ with T_s being calculated by

FLUENT. The only change in the problem was an additional specification in FLUENT for the inclusion of radiation. The same iterative procedure was used as described in Section 3.7

CHAPTER 4: NUMERICAL RESULTS

4.1 2-D Plane Wall Analysis Without Radiation

For the two-dimensional smooth wall analysis, an iterative procedure was implemented to determine the maximum amount of power each enclosure could dissipate while maintaining an approach temperature of 343 K. Aspect ratios of 1, 2, 3, 4, 6, 8, and 10 were analyzed. Table 4.1 provides a summary of the results. The most important result shown is how Q_{\max} varies with the enclosure aspect ratio. Note that for the two-dimensional configuration here, Q_{\max} has dimensions of W/m. Additionally, for each aspect ratio, several temperatures were recorded. These included the mean approach temperature near the bottom (T_b), enclosure surface temperature (T_s), the maximum temperature in the enclosure (T_m), and average plume temperature (T_p) located on the centerline, at a height above the heated elements of $0.25L$. Note that $T_b=343$ was a requirement in the analysis. The maximum temperature (T_m) occurred on the heater element surfaces. Figure 4.1 provides a graphical representation of the variation of Q_{\max} with aspect ratio, and Figure 4.2 provides the variation of key temperatures with aspect ratio.

Table 4.1: Effect of Aspect Ratio on Q_{\max} and Key Temperatures
(2-D, No Fins or Radiation)

AR	h (W/m ² K)	Q_{\max} (W/m)	T_b (K)	T_s (K)	T_m (K)	T_p (K)
1	5.53	49	343	327.6	369	363
2	4.76	77	343	330.4	377	366
3	4.36	104	343	332.3	384	370
4	4.1	131	343	333.6	391	373
6	3.75	183	343	335.5	404	379
8	3.51	229	343	336.4	414	382
10	3.35	281	343	337.9	426	390

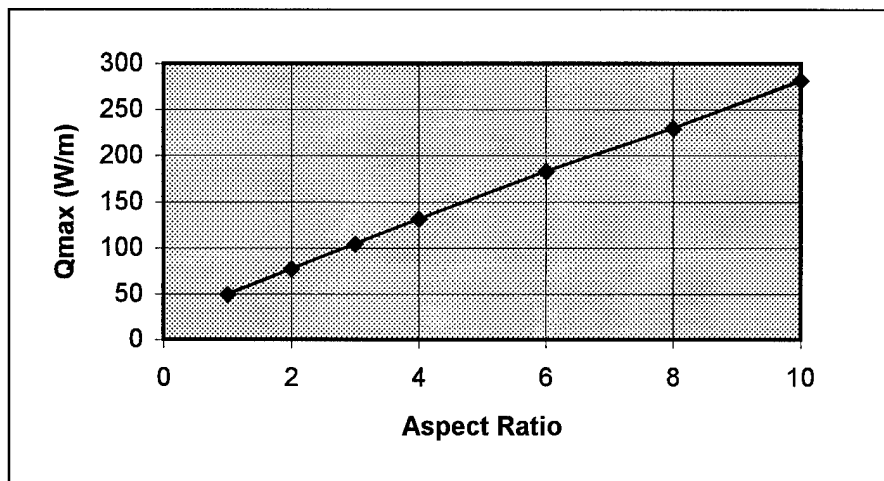


Figure 4.1: Q_{\max} Vs. Aspect Ratio
(2-D, No Fins or Radiation)

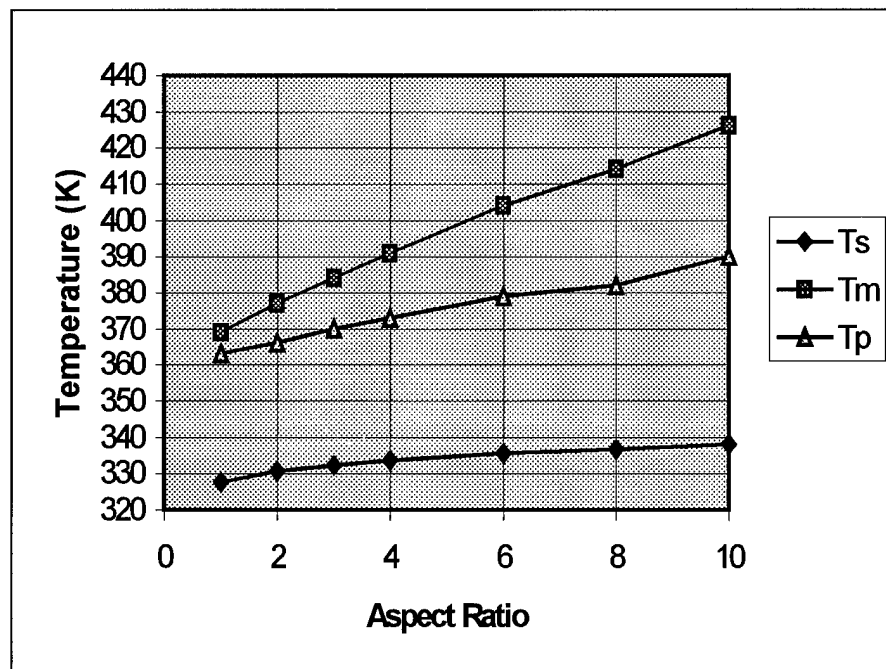


Figure 4.2: Key Temperatures Vs. Aspect Ratio
(2-D, No Fins or Radiation)

These results indicate that Q_{max} is roughly linear with aspect ratio. This is reasonable since enclosure surface area linearly increases as aspect ratio is increased. Apparently, the stack effect allows better circulation of the fluid as the height of the stack is increased. Additionally, another reason why Q_{max} appears to vary approximately linear with aspect ratio is that the “incomplete thermal penetration” regime is not observed. In other studies this region was observed when the volumetric heat generation was held constant while aspect ratio was varied. Furthermore, it is important to note that the approach temperature is 343 K, but the plume temperature directly above the heated region is significantly higher (375 K for AR=4).

4.2 2-D Smooth Wall With Radiation

The two-dimensional case is analyzed with the inclusion of radiation from the exterior surfaces. Internal radiation is not assumed to be an important transport mechanism since opposing surfaces are at the same temperature. The volumetric heat generation rate was adjusted until the desired approach temperature of 343 K was reached. All conditions remained the same except for the manipulation of the boundary condition in FLUENT. Now, instead of only external convection, the boundary condition was changed to accommodate combined external convection and radiation. The surface of the enclosure was given an emissivity of one, maximizing the radiation component. The same aspect ratios as for the two-dimensional plane wall without radiation were considered. Table 4.2 shows the variation of Q_{\max} and key temperatures with aspect ratio.

Figure 4.3 provides a graphical representation for the variation of Q_{\max} with aspect ratio and Figure 4.4 provides the variation of key temperatures.

TABLE 4.2: Effect of Aspect Ratio on Q_{\max} and Key Temperatures.
(2-D, With Radiation, No Fins)

AR	h (W/m K)	Q_{\max} (W/m)	T_b (K)	T_s (K)	T_m (K)	T_p (K)
1	5.04	72	343	318.4	375	366
2	4.3	126	343	320.5	390	371
3	4.08	192	343	323.2	408	383
4	3.73	242	343	323.7	417	385
6	3.52	373	343	325.5	444	398
8	3.2	486	343	326.2	464	403
10	3.14	641	343	328	492	420

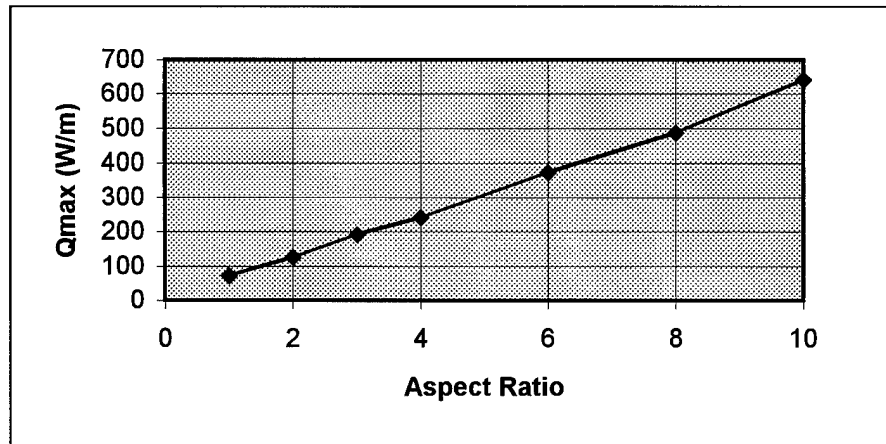


Figure 4.3 : Q_{\max} Vs. Aspect Ratio
(2-D, With Radiation, No Fins)

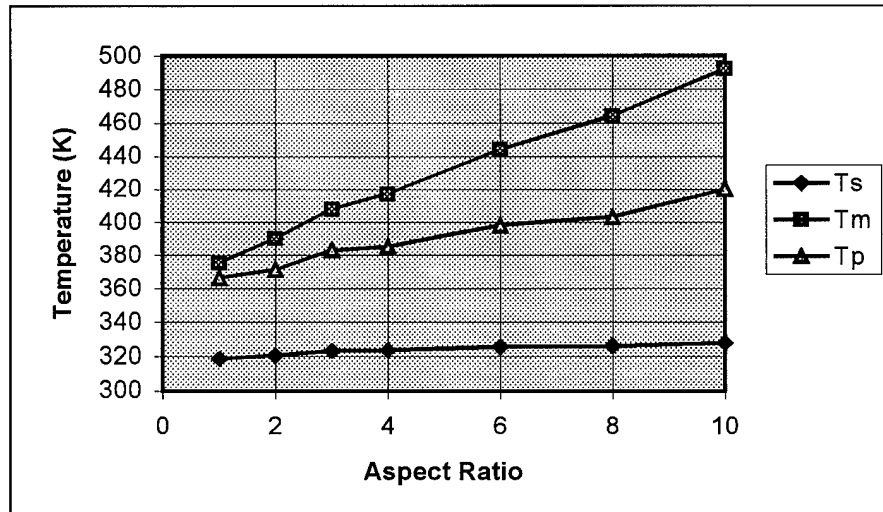


Figure 4.4: Key Temperatures Vs. Aspect Ratio
(2-D, With Radiation, No Fins)

Radiation is shown to have a major effect on heat rejection from plane wall enclosures. Results comparing the plane wall without radiation to the plane wall with radiation are presented in Chapter 5.

4.3 2-D Finned Wall Analysis

Fins were applied to the two dimensional case in order to observe their effect on enclosure cooling performance. External and internal fins were added, both having the same dimensions for the various cases considered. The fins were assumed to be made of aluminum and thus had efficiencies near 1.0. Fin spacing was varied between 0.4 cm and 2.0 cm, and fin height was varied between 1 cm and 5 cm. Note that a fin height of 5 cm would mean the interior fins on opposite walls would

touch. An enclosure having an aspect ratio of two was analyzed for each combination of fin spacing and height. Equation 3.18 was used in order to determine the external heat transfer coefficient. Table 4.3 provides a summary of the results for the Q_{\max} variation with fin geometry.

Table 4.3: Effect of Fin Geometry on Q_{\max} (W/m) for AR=2
(2-D, No Radiation)

Fin Height (cm)	Fin Spacing (cm)				
	0.4	0.8	1.2	1.6	2.0
1	128	136	144	140	*
2	202	198	187	187	*
3	252	230	219	209	*
4	229	237	227	229	*
5	*	*	*	*	179

For the configurations considered here it is seen that fin height has a much greater influence on the ability to reject heat than does fin spacing. For example, a fin spacing of 1.6 cm and a fin height of 1 cm exhibits 140 W/m of rejection. Now, if the fin spacing is halved (to 0.8 cm) and fin height held constant, which approximately doubles the fin area, the rejection changes little (136 W/m). On the other hand, if the spacing is held constant and the fin height is doubled to 2 cm (again doubling fin area), the rejection increases substantially (187 W/m). It is

important to note that it may be likely that above some critical fin height and fin spacing that each component will have the same effects.

The optimization of a fin geometry may be done on several objective functions. One might be: "What is the optimum fin configuration for maximizing heat rejection while maintaining fin material (volume) constant?" An example of this is shown by the shaded boxes, where the fin height/fin spacing equals 2.5. In this scenario, it is seen that the optimum fin configuration appears to be a spacing of about 1.6 cm, and a fin height of about 4 cm, resulting in a heat rejection of 229 W/m. This is shown in Figure 4.5 which shows heat rejection as a function of fin height for fin height/fin spacing equal to 2.5.

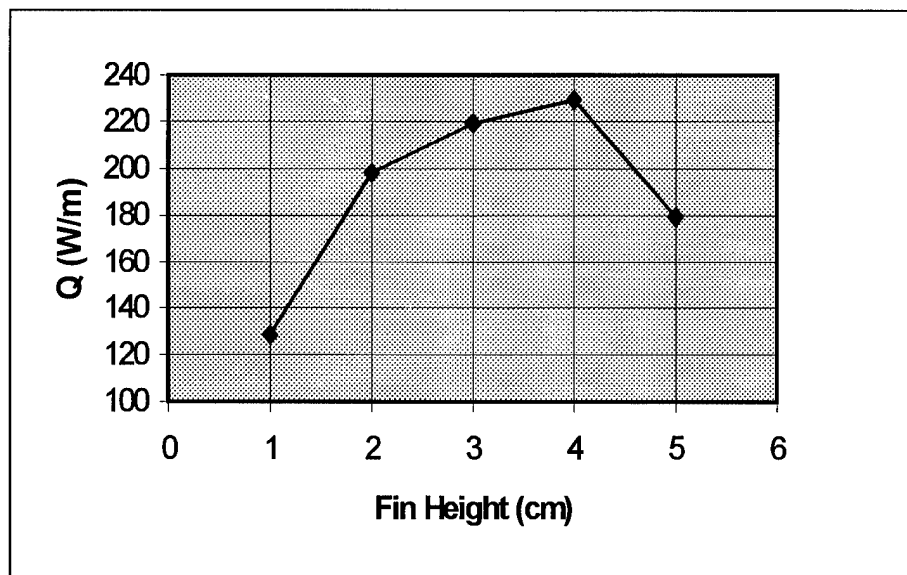


Figure 4.5: Heat Rejection as a Function of Fin Height For a Constant Height to Spacing Quotient and $AR=2$

The effect shown in Figure 4.5 can be attributed to the relative thickness of the boundary layer and the spacing. The shorter, densely packed fins do not allow the flow to penetrate between fins as the boundary layers overlap. A correlation from Incropera (1990), allows for the calculation of the boundary layer thickness on isothermal vertical walls. Using the surface temperatures taken from FLUENT output, the boundary layer thickness at $0.5L$ is approximately 1.1 cm for an enclosure height of 0.2m ($AR=2$). It is seen in Table 4.3 that a spacing of about 1.6 cm is needed to reach the maximum rejection, and this is consistent with being of the order of twice the boundary layer thickness. Figure 4.6 provides a graphical comparison between the shorter fins and the longer fins. As can be seen, the boundary layer overlaps more for the closely packed fins, thus preventing effective cooling from taking place.

One will notice from Table 4.3 that 252 W/m is the maximum amount of heat that can be dissipated in an enclosure with an aspect ratio of two, which is a bit larger than the optimum value of 229 W/m for fin height/spacing=2.5. However, due to the size and spacing of the fins, this configuration is much less desirable than one that can dissipate nearly the same amount of heat with a lower overall fin volume. The optimum configuration requires about 1/3 as much fin material as the configuration exhibiting 252 W/m of rejection.

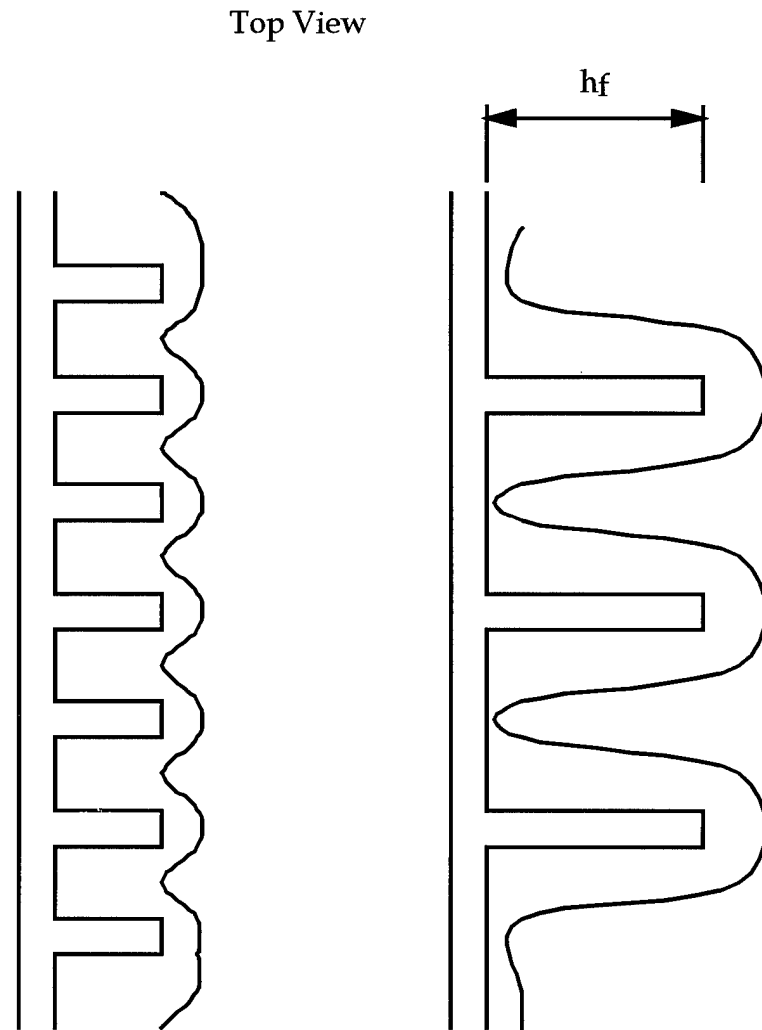


Figure 4.6: Boundary Layer Comparison for Configurations Having Comparable Fin Volume but Different Height and Spacing

FLUENT was also run for enclosure aspect ratios up to eight. For each aspect ratio, the optimum fin configuration was sought by finding the maximum heat rejection along the diagonal for which fin height/fin spacing is equal to 2.5. These results are summarized in Table 4.4,

where the values for Q_{opt} , optimum h_f , optimum b_f , and key temperatures are listed.

Table 4.4: Effect of Aspect Ratio on Q_{opt} and Key Temperatures
(2-D, Fins, No Radiation)

AR	h_{eff}	Q_{opt}	Opt h_f	Opt b_f	T_b	T_s	T_m	T_p
	W/m^2K	W/m	cm	cm	K	K	K	K
2	20.4	229	4	1.6	342.5	316.1	423	401
4	14	345	3	1.2	343	321.4	449	412
6	12.5	468	3	1.2	343	322.6	469	417
8	8.8	550	2	0.8	343	330.3	483	424

It was found that with increasing aspect ratio, the optimum fin configuration shifted to smaller height and spacing. Figure 4.7 provides a graphical representation of Q_{opt} versus aspect ratio, and Figure 4.8 provides a summary of the results for key temperatures versus aspect ratio for the optimum fin configurations.

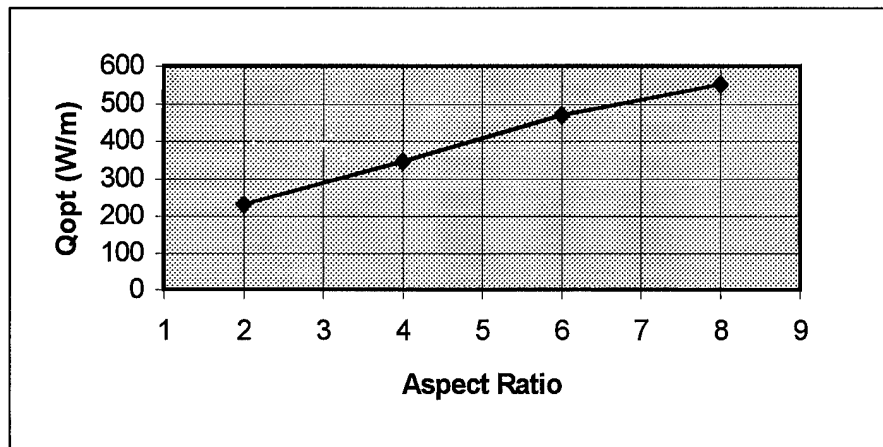


Figure 4.7: Q_{opt} Vs. Aspect Ratio
(2-D, Fins, No radiation)

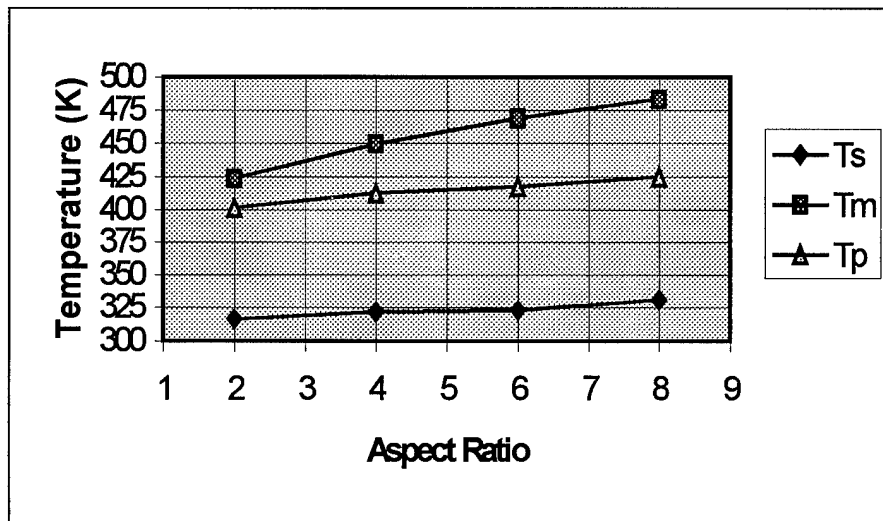


Figure 4.8: Key Temperatures Vs. Aspect Ratio
(2-D, Fins, No Radiation)

The application of fins is shown to have significant effects on heat rejection from enclosures. Results comparing the plane wall without radiation to the finned wall are presented in Chapter 5.

4.4 2-D Finned Wall With Radiation

Radiation on the exterior surfaces may be considered with fin geometries as was discussed in the earlier analysis for plane enclosure walls. Again, internal radiation is neglected. The optimal fin spacing geometries were used, and enclosure wall emissivity was set at one. The power dissipated and key temperatures for combined radiation and finning, at aspect ratio's of 2, 4, 6, and 8, are summarized in Table 4.5

Table 4.5: Effect of Aspect Ratio on Q_{opt} and Key Temperatures (2-D, Fins and Radiation)

AR	h_{eff} (W/m ² K)	Q_{opt} (W/m)	T_b (K)	T_s (K)	T_m (K)	T_p (K)
2	19	274	342.5	314.4	432	406
4	13.1	461	343	318.2	468	422
6	11.8	648	343	319.1	500	433
8	8.1	864	343	324.9	531	443

Figure 4.9 provides a graphical representation of Q_{opt} versus aspect ratio and Figure 4.10 provides a summary of the results for key temperatures versus aspect ratio.

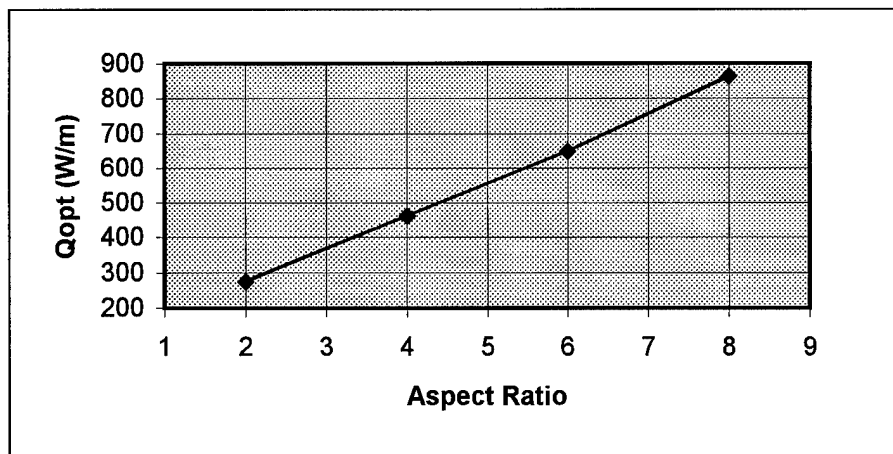


Figure 4.9: Q_{opt} Vs. Aspect Ratio
(2-D, Fins and Radiation)

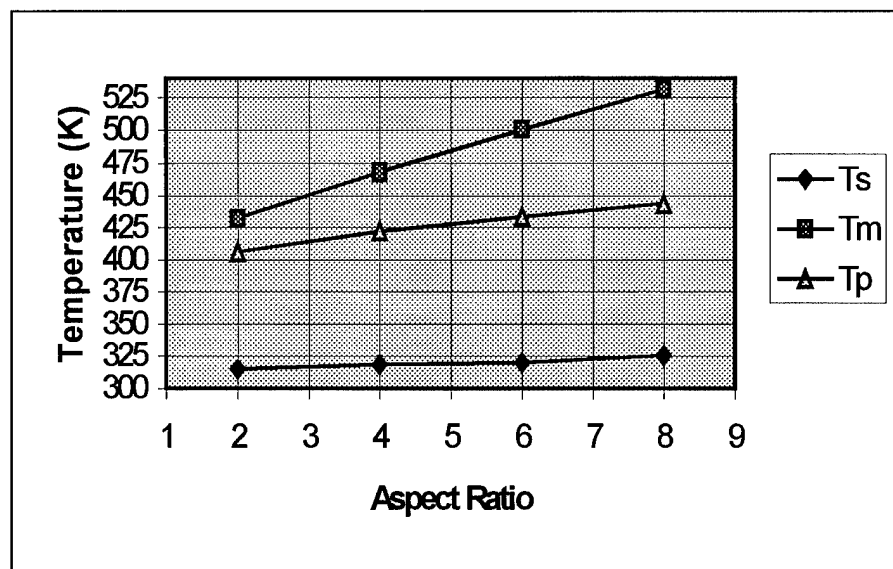


Figure 4.10: Key Temperatures Vs. Aspect Ratio
(2-D, Fins and Radiation)

The combination of fins and radiation increases the amount of heat dissipation substantially, and these effects are nearly additive. Chapter 5 provides further discussion on these results.

4.5 3-D Plane Wall Analysis Without Radiation

An analysis was conducted for the three dimensional case for comparison with the two-dimensional case. The aspect ratios were varied and the volumetric heat generation rate was increased until an approach temperature of 343 K was reached. The external heat transfer coefficient for the three-dimensional case is governed by Equation 3.7. Aspect ratios of 1, 2, 3, and 10 were studied. Most runs were for lower aspect ratios for several reasons. First, as Shen reported, aspect ratios of more than three had minimal effect on maximum temperature. It was initially believed that this might also apply for the mean approach temperature. Furthermore, lower aspect ratios were chosen because of the shorter convergence time needed for FLUENT to solve the more complex three-dimensional problems. A value of 10 was chosen so that a better trend could be determined. Table 4.6 shows the pertinent data from this analysis.

Table 4.6: Effect of Aspect Ratio on Q_{\max} and Key Temperatures (3-D, No Fins or Radiation)

AR	h (W/m ² K)	Q_{\max} (W)	T_b (K)	T_s (K)	T_m (K)	T_p (K)
1	5.6	8.64	343	330.9	379	364
2	4.82	14.7	343	334.1	397	371
3	4.43	20.9	343	335.6	413	378
10	3.44	62	343	344.2	523	414

Figure 4.11 provides a graphical representation of Q_{\max} versus aspect ratio and Figure 4.12 provides a summary of the results for key temperatures versus aspect ratio.

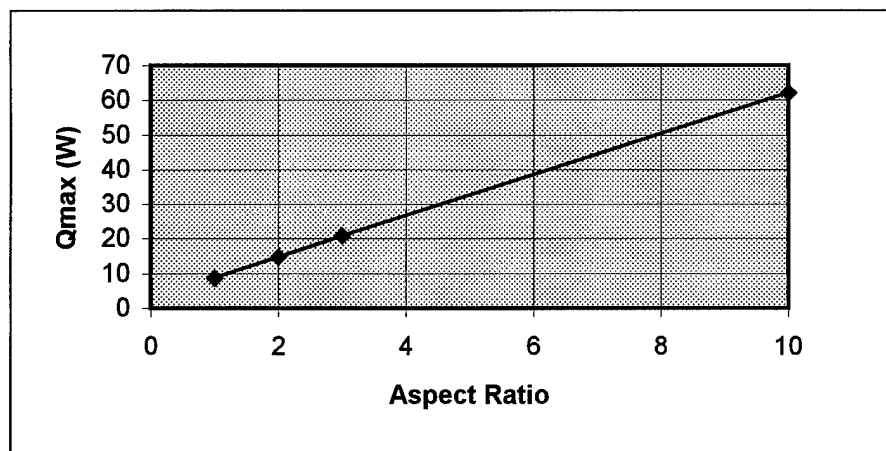


Figure 4.11: Q_{\max} Vs. Aspect Ratio
(3-D, No Fins or Radiation)

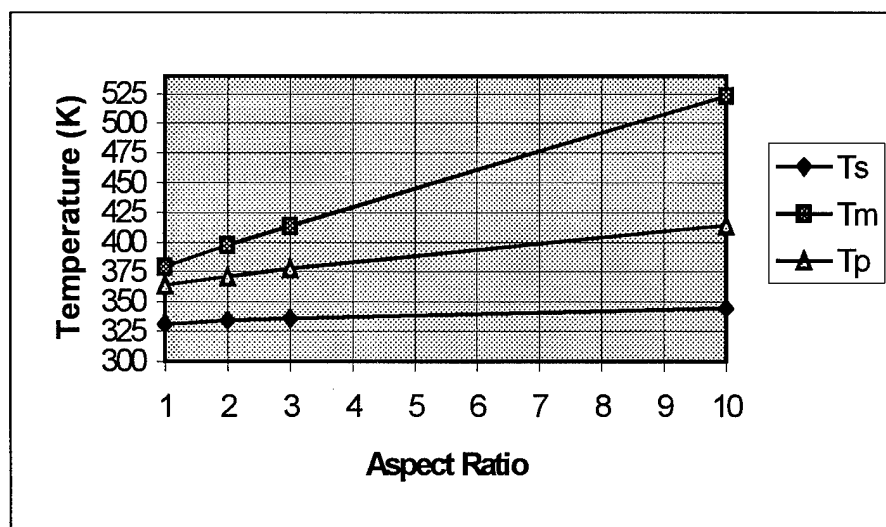


Figure 4.12 Key Temperatures Vs. Aspect Ratio
(3-D, No Fins or Radiation)

The three-dimensional results are compared with the two-dimensional results in Chapter 5.

4.6 2-D Heater Element Size Effects

A question arising in this analysis is: "Does the heater configuration significantly influence the results?" For example, very narrow fluid passages between elements could restrict the flow and alter the permissible heat dissipation. Therefore, the thicknesses of the heater elements located in the bottom of the enclosure were varied from 0.2 cm to 0.6 cm, to both increase and decrease the fluid passage width. One case was run using only two elements, each 0.4 cm by 3 cm to minimize fluid resistance. This analysis was done for an enclosure aspect ratio of two, and for plane walls without radiation. Table 4.7 summarizes the results, and it is seen that there is relatively little influence on the allowable heat dissipation as the heater configuration is varied.

Table 4.7: Q_{\max} Vs. Heater Element Thickness

Number of Heaters	Heater Element Thickness (cm)	Q_{\max} (W/m)
6	0.2	95
6	0.4	93
6	0.6	91
2	0.4	98

CHAPTER 5: COMPARISONS & DISCUSSION

5.1 2-D Comparisons

Table 5.1 compares the relative contributions of finning and radiation toward the amount of power an enclosure is able to dissipate without exceeding the safe approach temperature of 343 K. Percent differences are relative to the base case.

Table 5.1: Comparison of Q_{\max} Values for 2-D Cases

AR	Base Case	Rad Only	Increase	Fin Only	Increase	Rad & Fin	Increase
	W/m	W/m	%	W/m	%	W/m	%
2	77	126	64	229	197	274	256
4	131	242	85	345	163	461	252
6	183	373	104	468	156	648	254
8	229	486	112	550	140	864	277

Table 5.1 shows that radiation exhibits a relatively greater influence on cooling performance for larger aspect ratios. The percent increase in the allowable heat dissipated ranges from 64% for an aspect ratio of 2, to 112% for an aspect ratio of 8. A reason for this is that enclosure surface temperatures increase as aspect ratio increases.

Conversely, finning the enclosure surface is less influential at higher aspect ratios. The percent increase in the amount of heat that can be dissipated ranges from 197% for an aspect ratio of 2, to 140% for an aspect ratio of 8, which exceeds the enhancement due to radiation alone. One might expect this variation for fins since the area for heat transfer becomes more limited with decreasing aspect ratios. It is also shown that the effects of radiation and finning are nearly additive. Furthermore, for combined radiation and finning the percent increase in heat dissipated from the enclosure, over that of a plane enclosure without radiation, is relatively constant as a result of the counterbalancing effects of radiation and finning.

All the two-dimensional cases that are analyzed appear to follow a nearly linear variation of heat dissipation with aspect ratio. This is reasonable since enclosure surface area is linearly increased as aspect ratio is increased. Figure 5.1 shows this relationship for the various design combinations. It is seen that although finned walls generally dissipate more heat than plane walls with radiation, this difference decreases with aspect ratio.

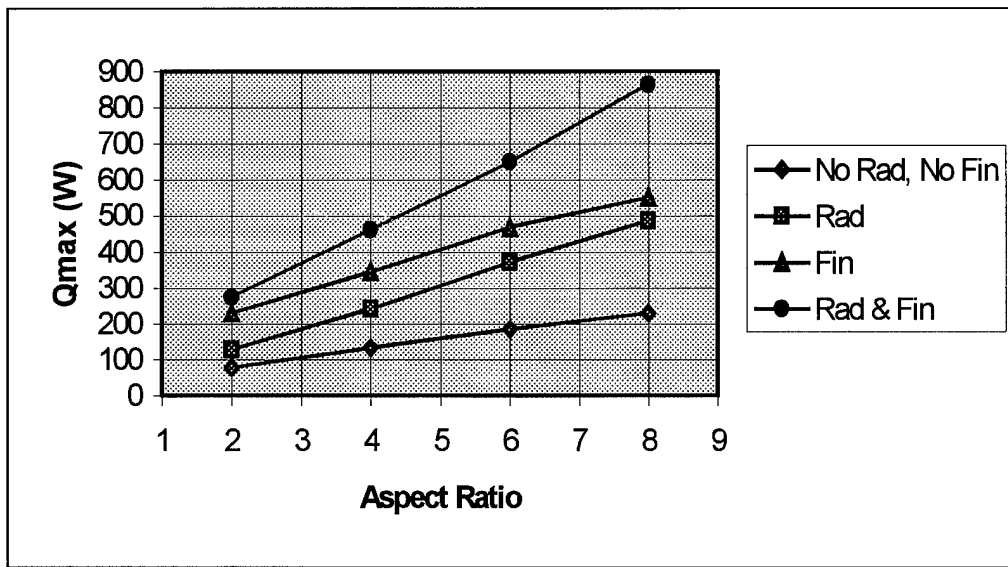


Figure 5.1: Comparison of Power Dissipation with Aspect Ratio for Various 2-D Cases

Figures 5.2 through 5.4 show how each of the key temperatures for the different designs vary with aspect ratio.

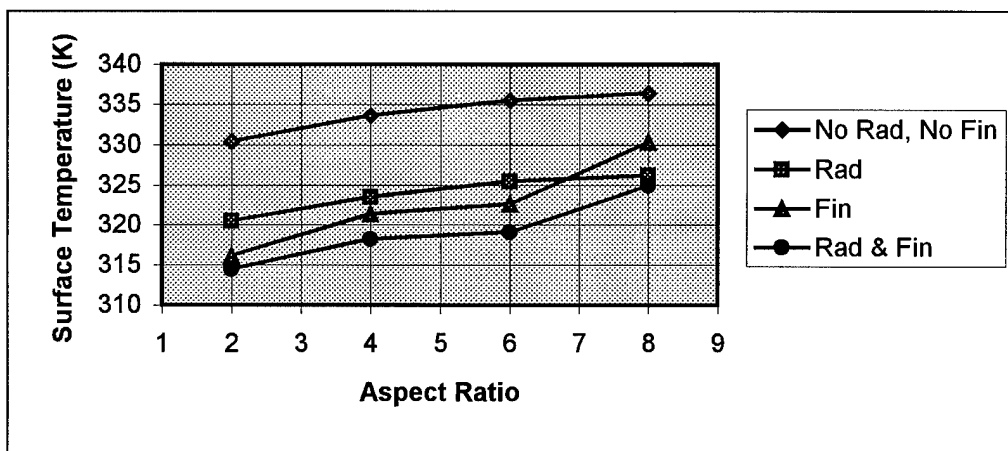


Figure 5.2: Enclosure Surface Temperature Vs. Aspect Ratio

Surface temperatures for the non-finned cases (Figure 5.2) appear to increase rather steadily until an aspect ratio of 6 is reached, and then they begin to level off. For the finned cases the surface temperatures increase until $AR=4$, level off from $AR=4$ to $AR=6$, and then increase more rapidly for aspect ratios greater than 6. No explanation is offered for this behavior at the present time.

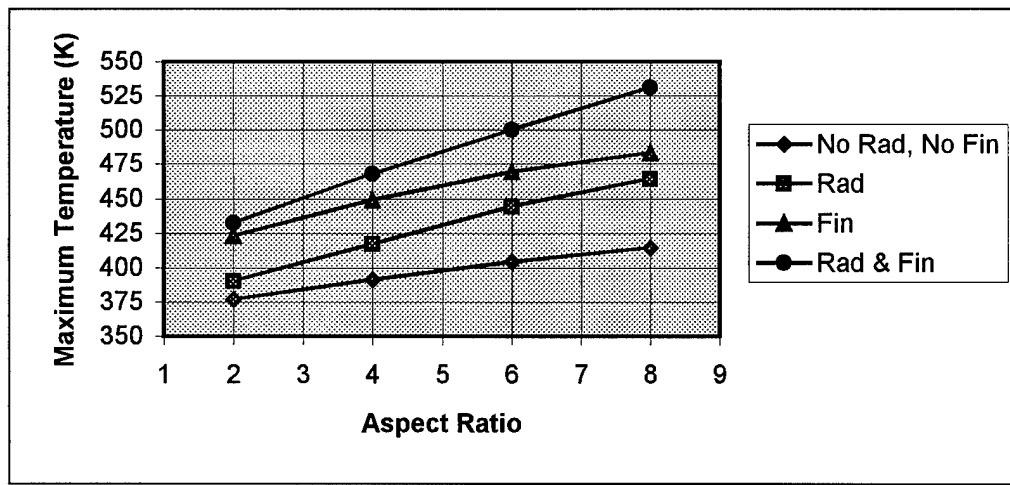


Figure 5.3: Maximum Temperature Vs. Aspect Ratio

The maximum temperatures (Figure 5.3) exhibit a fairly linear variation with aspect ratio, similar to that seen for the variation of maximum heat rejection with aspect ratio (Figure 5.1). It is important to note that the maximum temperatures are always found within the heater elements furthest from the center of the enclosure. This becomes important to designers as they must take into consideration the maximum allowable temperature of circuit boards.

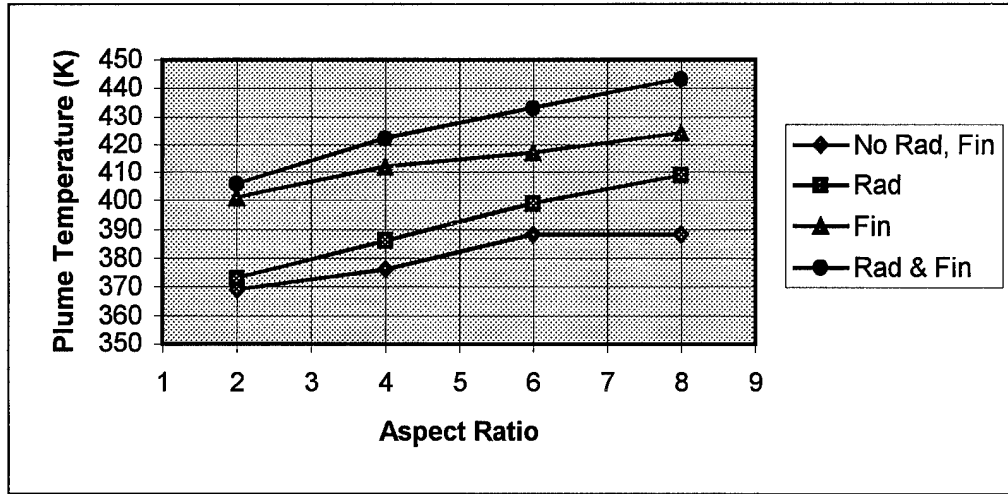


Figure 5.4: Plume Temperature Vs. Aspect Ratio

The importance of the plume temperature is that it represents the environment temperature for the upper portion of the heated elements. While the approach temperature is always kept at 343 K, plume temperatures above the heated elements are found to be as high as 440 K (Figure 5.4). This large fluid temperature increase across the heated region warrants consideration from designers as components in the upper portion of circuit boards may be damaged by excessive temperatures, even though the approach temperature is within specifications.

5.2 2-D & 3-D Comparison

Comparisons are made between the two-dimensional and three-dimensional cases for a plane wall without radiation for aspect ratios of

1, 2, 3, and 10. Heat dissipation for the two-dimensional cases are given in W/m and in watts for the three dimensional cases. They are both converted to W/m^2 (of enclosure area) for comparison, by taking into account their respective enclosure surface areas. Table 5.2 shows the results.

Table 5.2: Comparison of the Heat Rejection per Unit Area of Enclosure for 2-D and 3-D Cases

AR	2-D Case W/m^2	3-D Case W/m^2	Percent Difference
1	163.3	172.8	5.8
2	154	163.3	6.0
3	148.6	161.1	8.4
10	133.8	147.2	10.0

The results for the two-dimensional and three-dimensional cases are very similar considering the different geometries. The percent differences in power dissipation between the three-dimensional and two-dimensional cases vary from 5.8% to 10% relative to the two-dimensional case. The differences will actually be slightly larger because the external heat transfer coefficients calculated for the three-dimensional cases assumed infinitely wide plane walls.

5.3 FLUENT Temperature and Contour Plots

Appendix A contains the two-dimensional temperature contour plots for aspect ratios of 1, 2, 3, 4, 6, 8, and 10. They indicate that the majority of the enclosure interior remains nearly isothermal, while strong temperature gradients are found near the walls of the enclosure, and bottom of the cavity. This is similar to the results reported by Ganzarolli and Milanez as discussed in Chapter 1.

Appendix B shows the two-dimensional velocity contour plots for the same aspect ratios as for temperatures. The highest velocities are found near the enclosure walls, as the fluid in contact with the enclosure walls is cooled. Due to the nature of the velocity characteristics of the thermosyphon flow field, the heated elements furthest from the center have the highest temperature found within the enclosure. These elements lie in regions of near zero velocities where little circulation or cooling occurs. Figure 5.5 shows a typical velocity profile at a location of $0.25L$ above the heaters. Notice how the region of zero velocity is in the approximate location of the heaters farthest from the center.

Appendix C contains the temperature contour plots for all cases, except the plane wall without radiation (Appendix A), with an aspect ratio of 2. Since symmetry was used for cases run with fins, only half of the enclosure is seen. Cases include plane wall with radiation, finned walls with plots taken near the fin (one computational cell away) and

halfway between fins, finned walls with radiation near fins and between fins, and a three-dimensional plane wall case taken at the mid-plane.

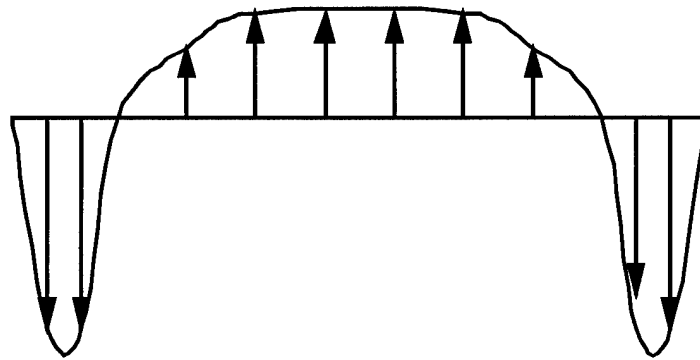


Figure 5.5: Velocity Profile Above Heaters ($0.25L$)

One may discern the impact of the different conditions on the temperature contours.

Appendix D follows the same format as Appendix C, but contains velocity plots rather than temperature plots. One will notice by comparing Appendix D.2 and D.3 that the near-wall velocity is effected considerably by the fins. Velocities are approximately 0.07 m/s near the fin compared to 0.18 m/s at the mid-plane between fins.

CHAPTER 6: CONCLUSION & RECOMMENDATIONS

6.1 Conclusion

Numerical studies using FLUENT have provided information regarding the heat rejection capability of a natural convection/thermosyphon device. Configurations that were analyzed included the plane wall with and without radiation, and finned walls with and without radiation. Heat rejection for all configurations was almost linear with aspect ratio (enclosure area). For the plane wall the relative contribution of radiation to the heat rejection increased with aspect ratio, varying from 64% to 112%. The optimally finned wall exhibited lower relative contribution with increasing aspect ratio, that contribution varying from 197% to 140%. In general, the finned surfaces provided better enhancement than did radiation. The optimally finned wall with radiation increased cooling performance by 252% to 277% over the range of aspect ratios considered. It was also shown that the maximum heat rejection for the two-dimensional geometry was in close agreement with the three-dimensional geometry, differing only by 5.8% to 10%. Heater element configuration was shown to have a small effect on cooling performance.

6.2 Recommendations

The numerical simulation performed here should be extended to provide a better understanding of the trends and factors effecting the cooling performance of enclosures. Areas for consideration include further simulations, experimental validation, and the determination of an appropriate correlation.

In this numerical simulation cavity width was held constant at 10 cm. It would be beneficial to run additional simulations with FLUENT for a range of cavity widths (4 cm to 20 cm) to better understand the effects of geometry on electronic component cooling. Another parameter for variation would be fin material. The external heat transfer coefficients found in this study are quite low (of the order of 3 to 5 W/m²K). The result is that the efficiency is of the order of 30% to 50%. The analysis should be extended to more accurately simulate plastic fin material, as such materials may be cheaper and the components more easily fabricated. Additionally, it is recommended that extended simulations of the three-dimensional geometry, and cylindrical geometries be performed to compare with the two-dimensional results. One configuration may prove significantly better than the other. Furthermore, some limited simulations of complete geometries (interior and exterior) would better assure that the heat transfer on the external surface is being treated correctly. Finally, it might be beneficial to observe plume temperature (T_p) more closely, as

the upper portion of the heated elements are exposed to relatively high temperatures.

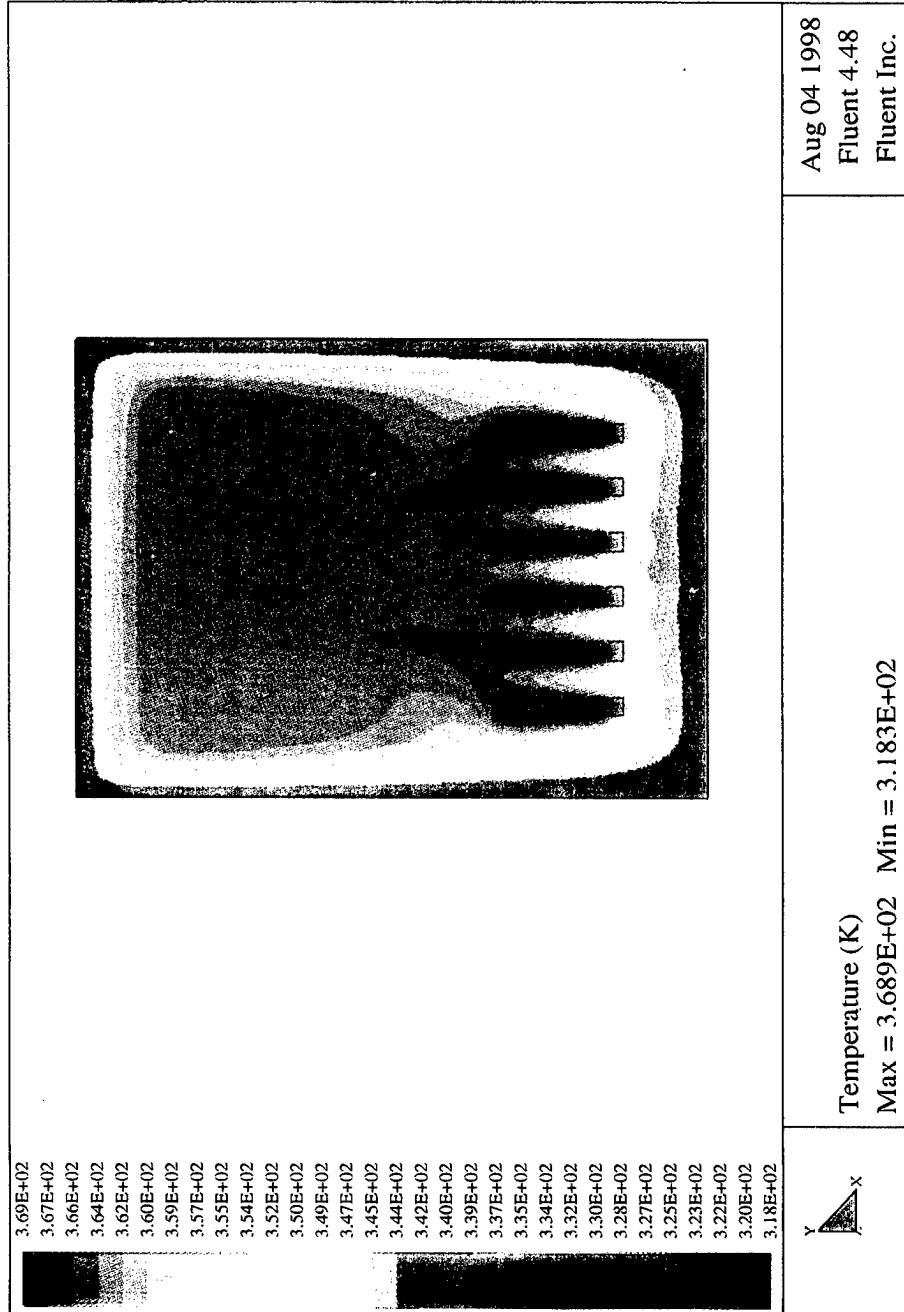
Experiments should also be conducted to validate the numerical simulations. These studies should examine different fin materials and enclosure geometries. For two-dimensional geometries, the experimenter must ensure that the cavity depth (D) is large enough, relative to the cavity width (W), so as to minimize end effects.

Finally, with the results from both experimental and numerical simulations, a correlation should be derived for determining the optimum enclosure characteristics for heat dissipation from electronic components. This correlation should take into account factors such as enclosure geometry, fin geometry, radiation effects, and heated element configuration.

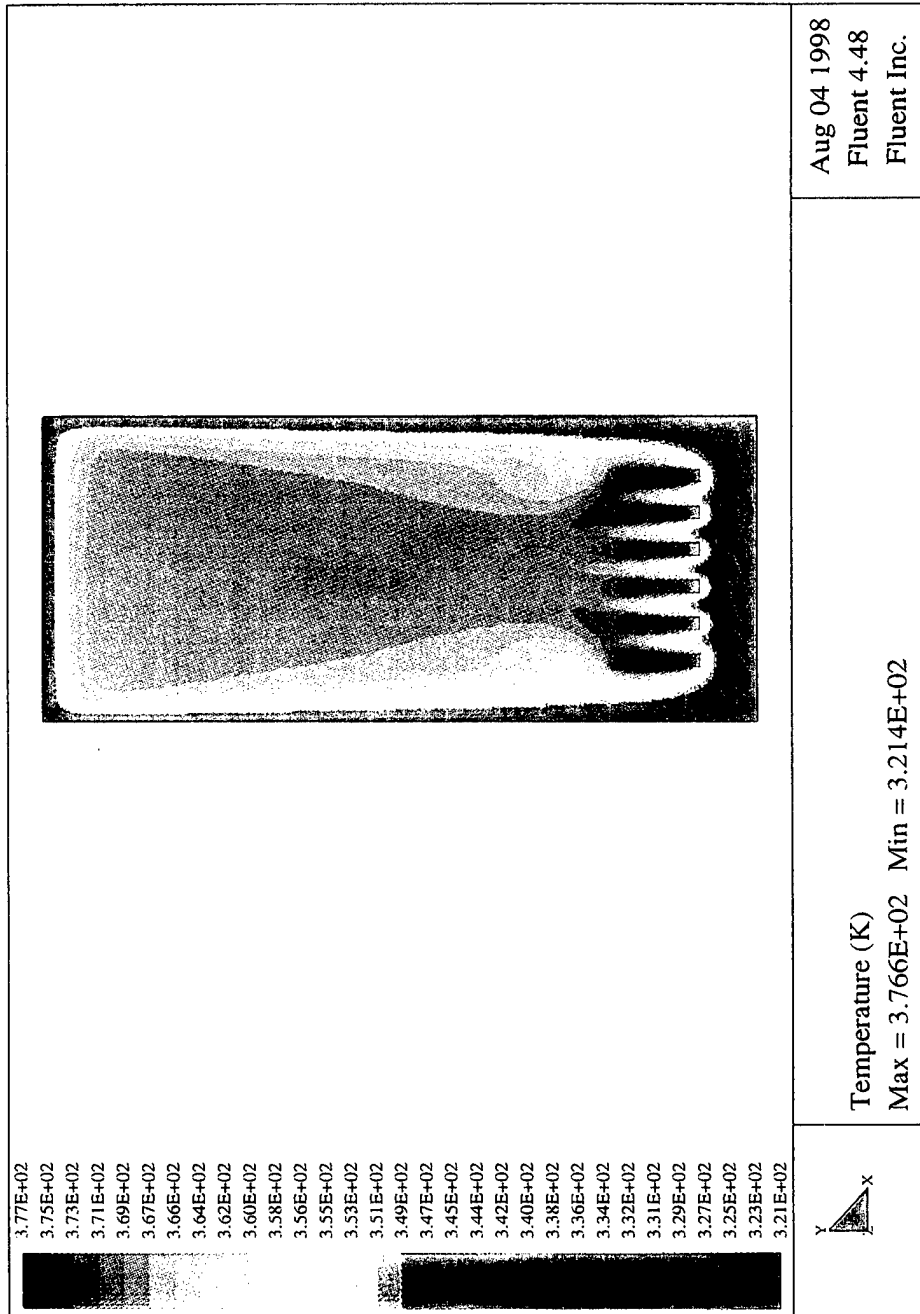
APPENDIX A:

2-D PLANE WALL TEMPERATURE CONTOUR PLOTS

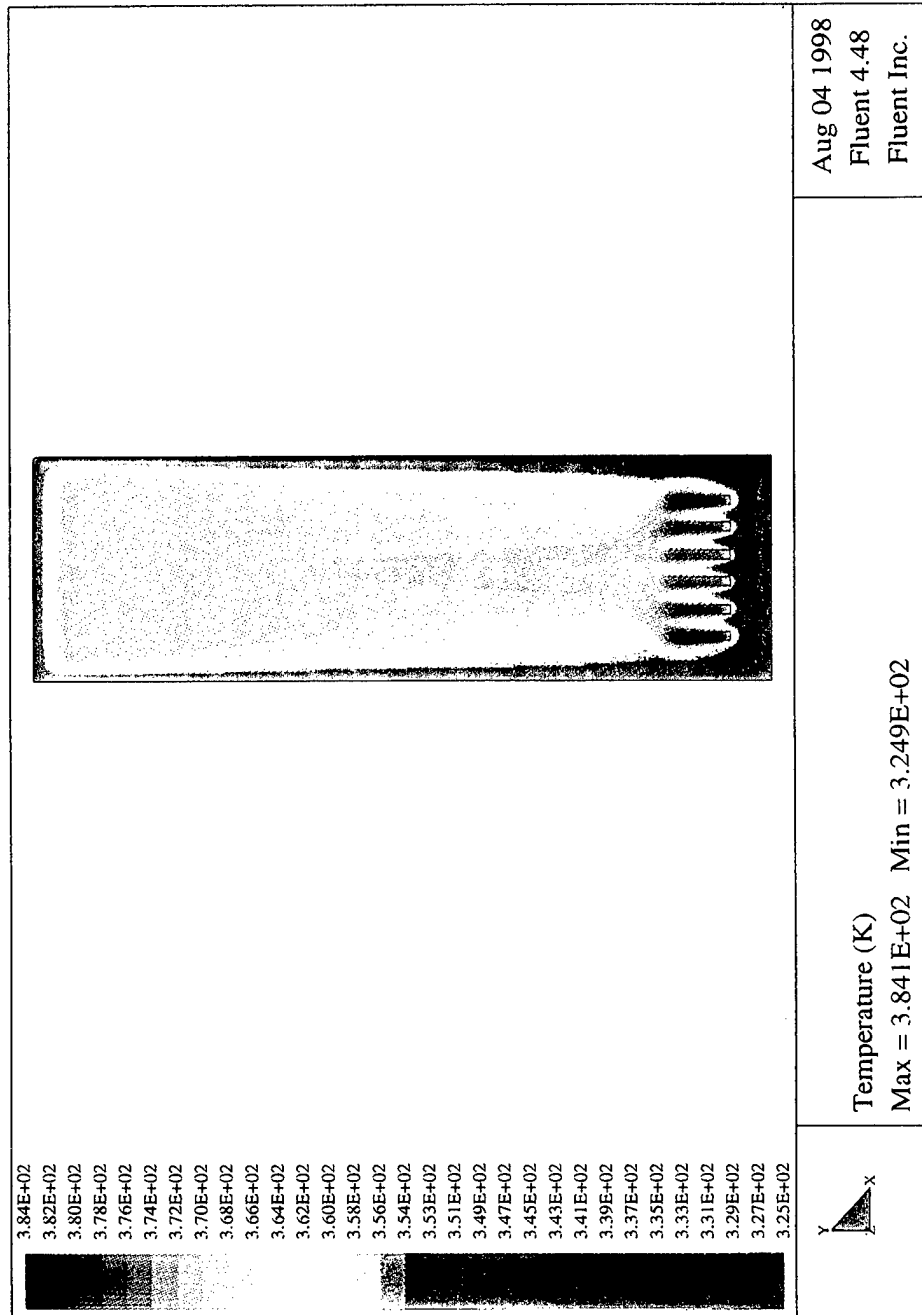
A.1: AR=1



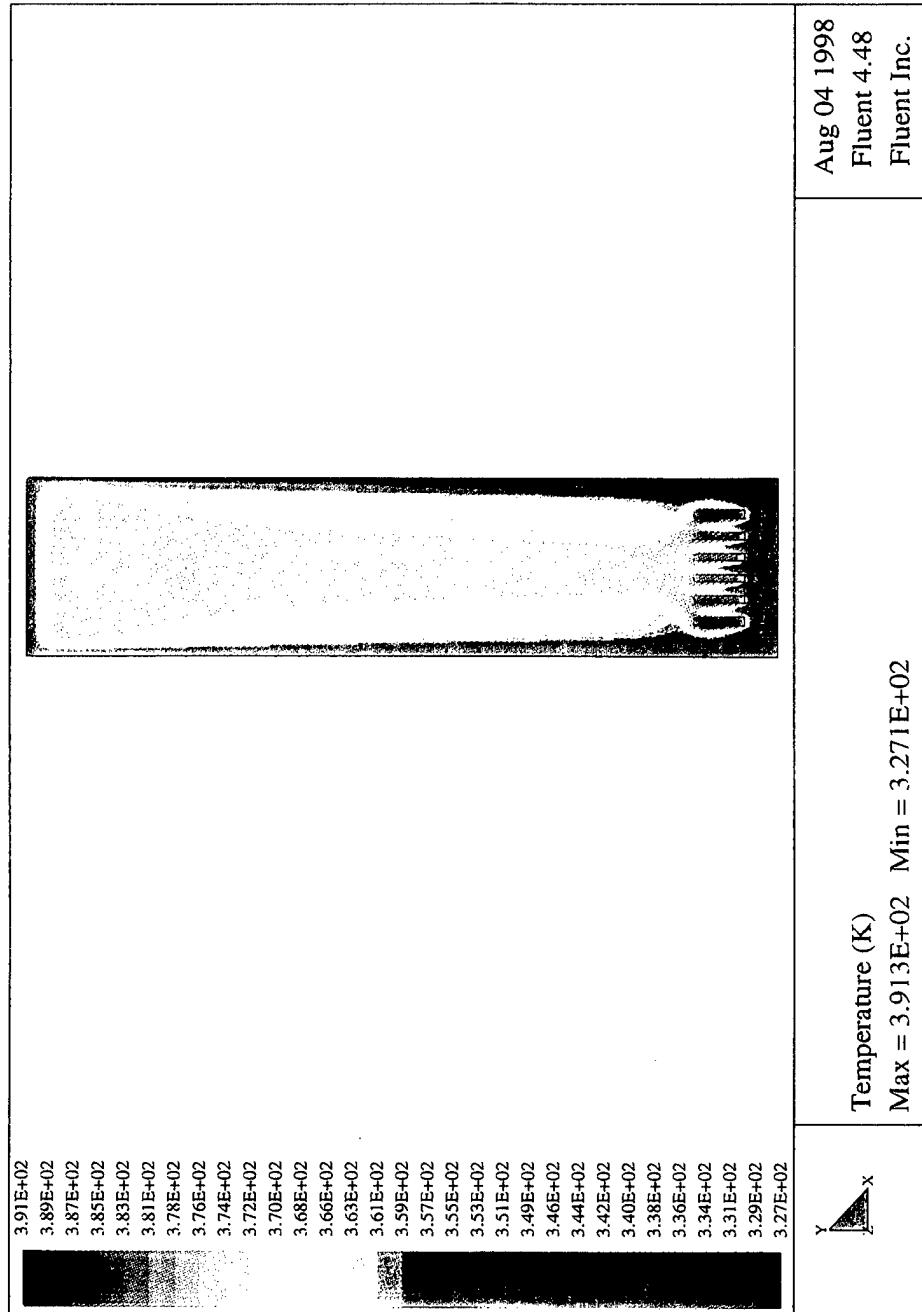
A.2: AR=2



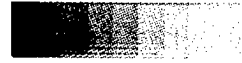

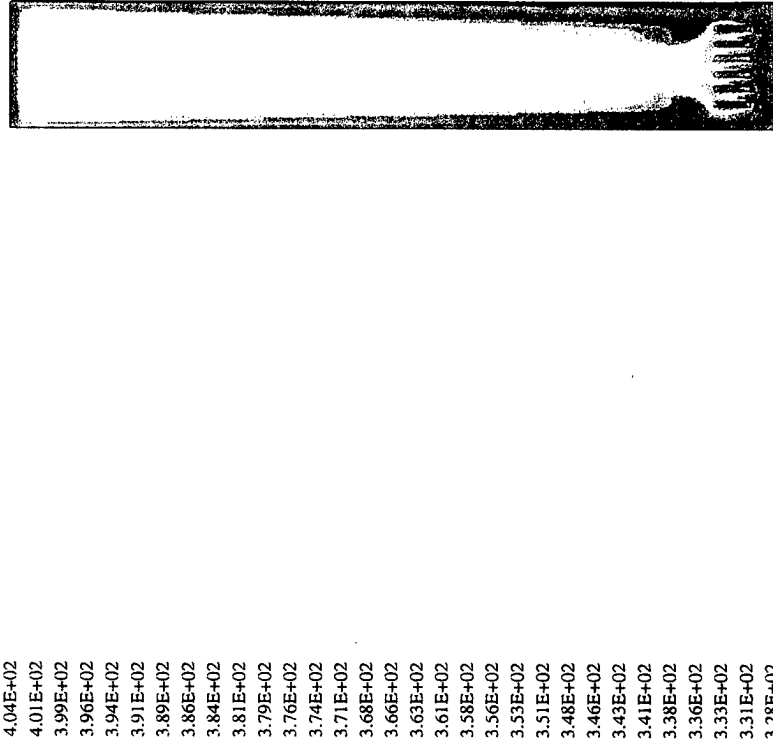

A.3: AR=3



A.4: AR=4



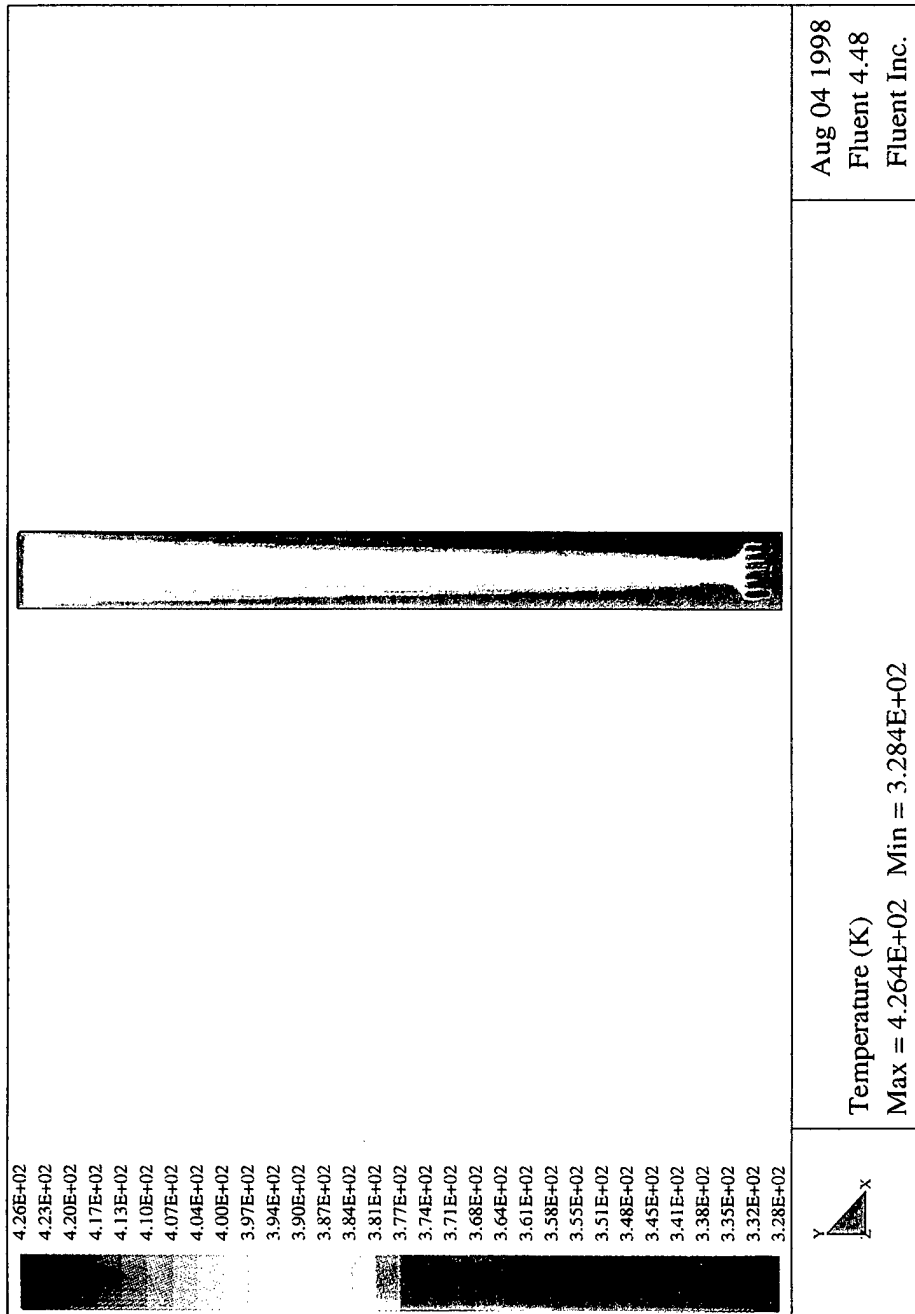
A.5: AR=6

 		<div data-bbox="1138 1556 1203 1623">  </div> <div data-bbox="1170 1041 1242 1501"> <p>Temperature (K) Max = 4.039E+02 Min = 3.280E+02</p> </div> <div data-bbox="1133 401 1242 564"> <p>Aug 04 1998 Fluent 4.48 Fluent Inc.</p> </div>
--	---	---

A.6: AR=8

<div data-bbox="344 1675 1107 1732" data-label="Figure"> </div> <div data-bbox="344 1585 1107 1669" data-label="Text"> <p>4.14E+02 4.11E+02 4.08E+02 4.05E+02 4.02E+02 3.99E+02 3.96E+02 3.93E+02 3.91E+02 3.88E+02 3.85E+02 3.82E+02 3.79E+02 3.76E+02 3.73E+02 3.71E+02 3.68E+02 3.65E+02 3.62E+02 3.59E+02 3.56E+02 3.53E+02 3.50E+02 3.48E+02 3.45E+02 3.42E+02 3.39E+02 3.36E+02 3.33E+02 3.30E+02 3.27E+02</p> </div> <div data-bbox="344 949 1107 1045" data-label="Figure"> </div>	<div data-bbox="1123 1554 1240 1732" data-label="Figure"> </div> <div data-bbox="1123 1081 1240 1543" data-label="Text"> <p>Temperature (K) Max = 4.136E+02 Min = 3.275E+02</p> </div> <div data-bbox="1123 436 1240 619" data-label="Text"> <p>Aug 04 1998 Fluent 4.48 Fluent Inc.</p> </div>
--	--

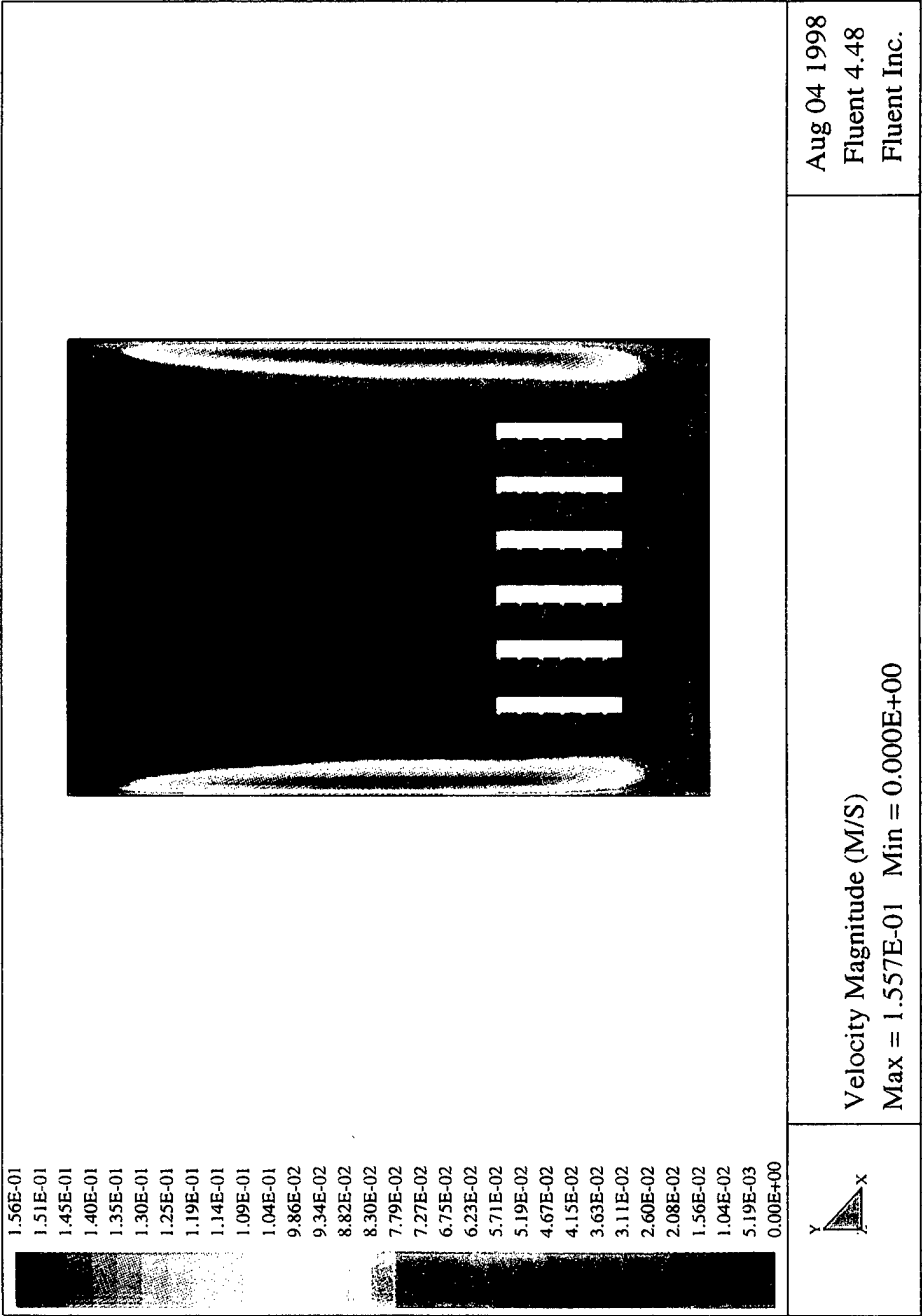
A.7: AR=10



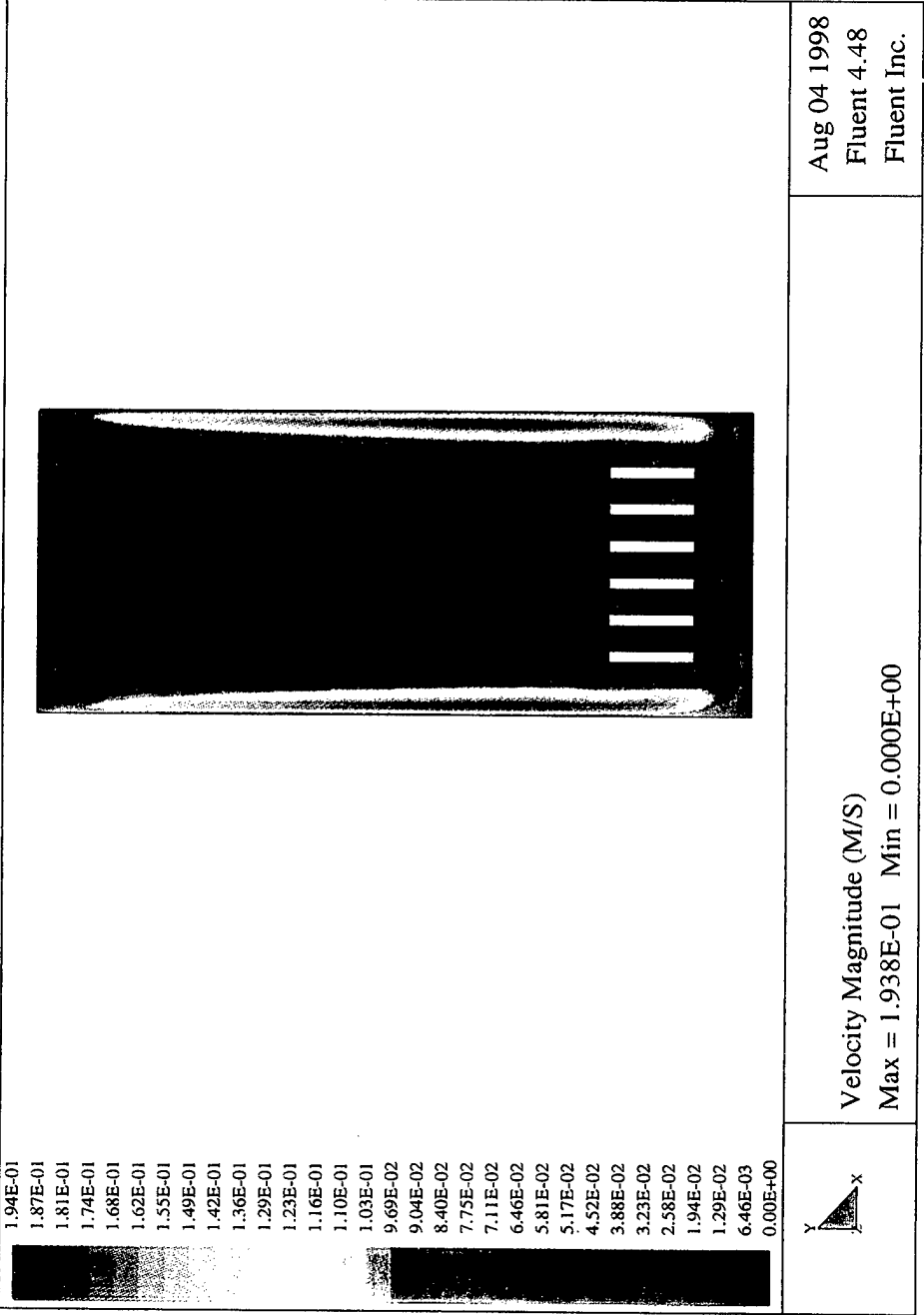
APPENDIX B:

2-D PLANE WALL VELOCITY CONTOUR PLOTS

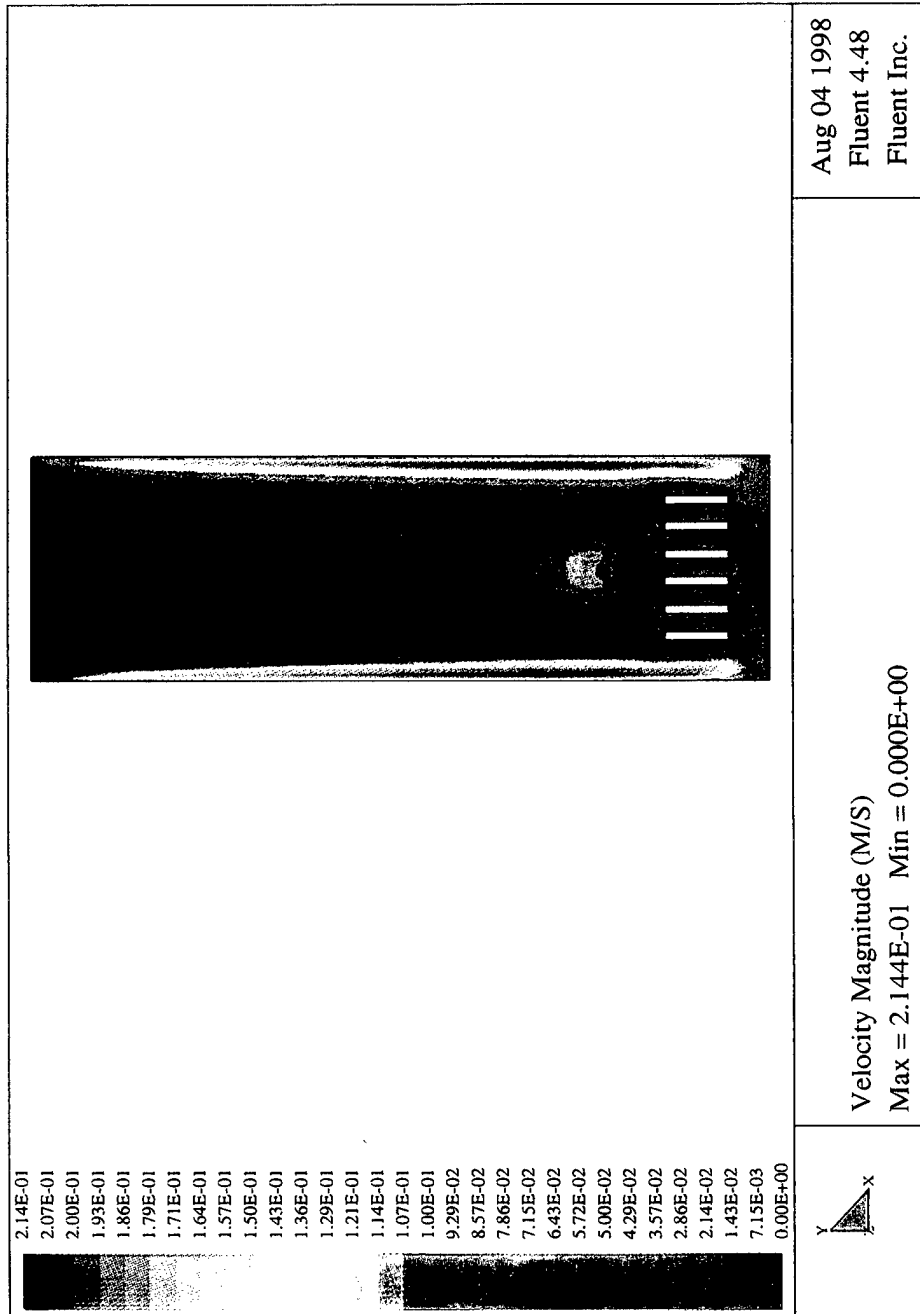
B.1: AR=1



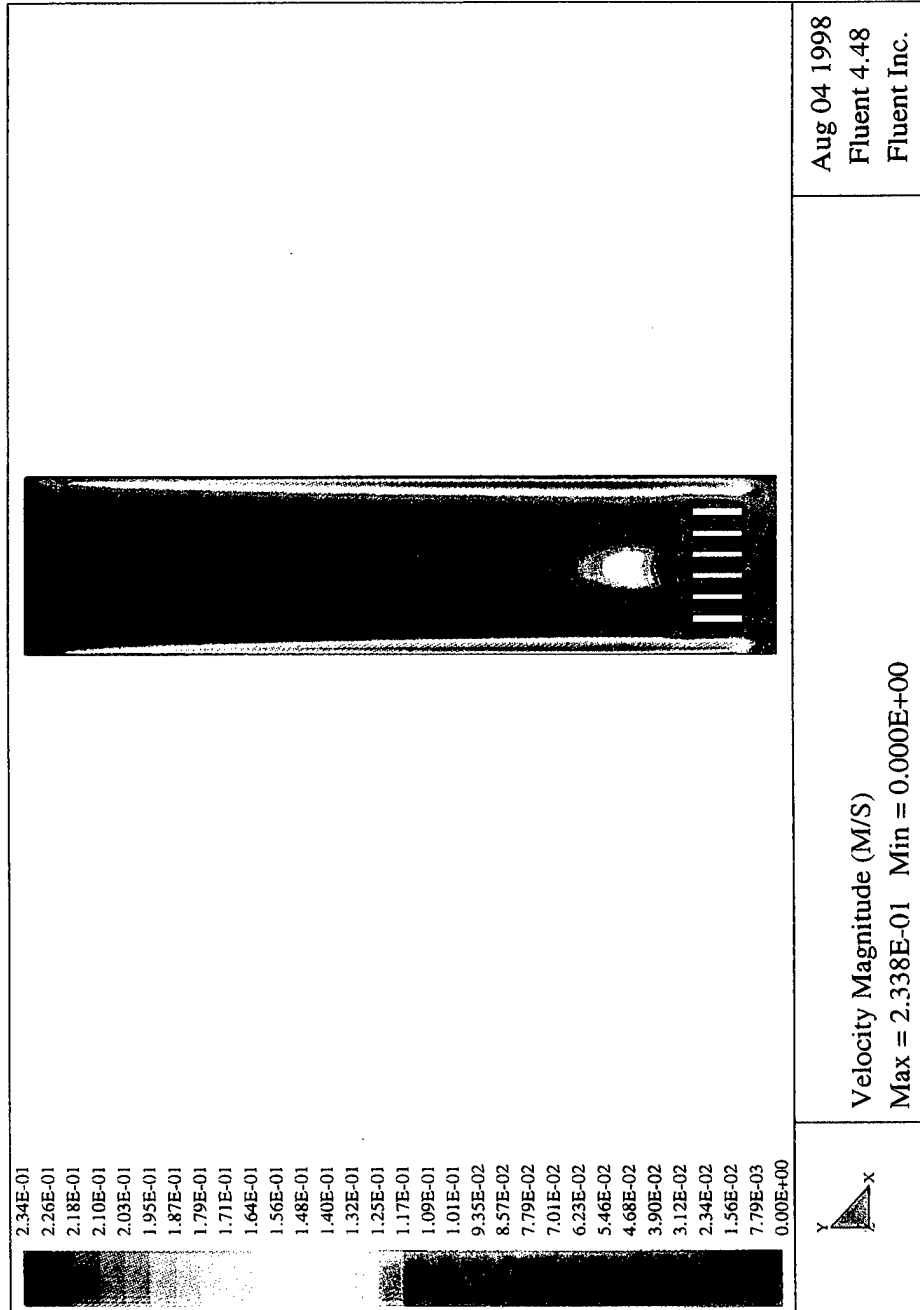
B.2: AR=2



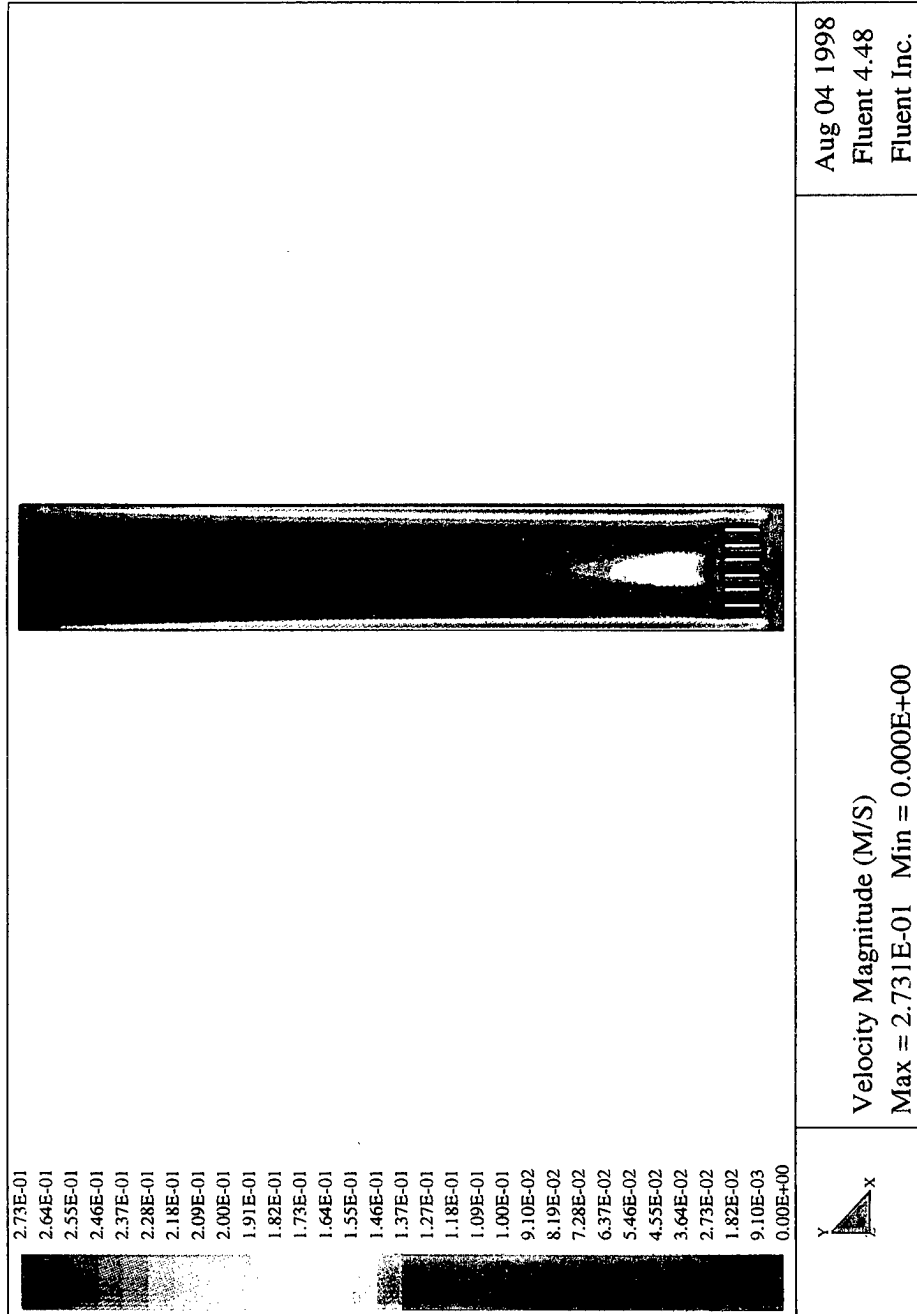
B.3: AR=3



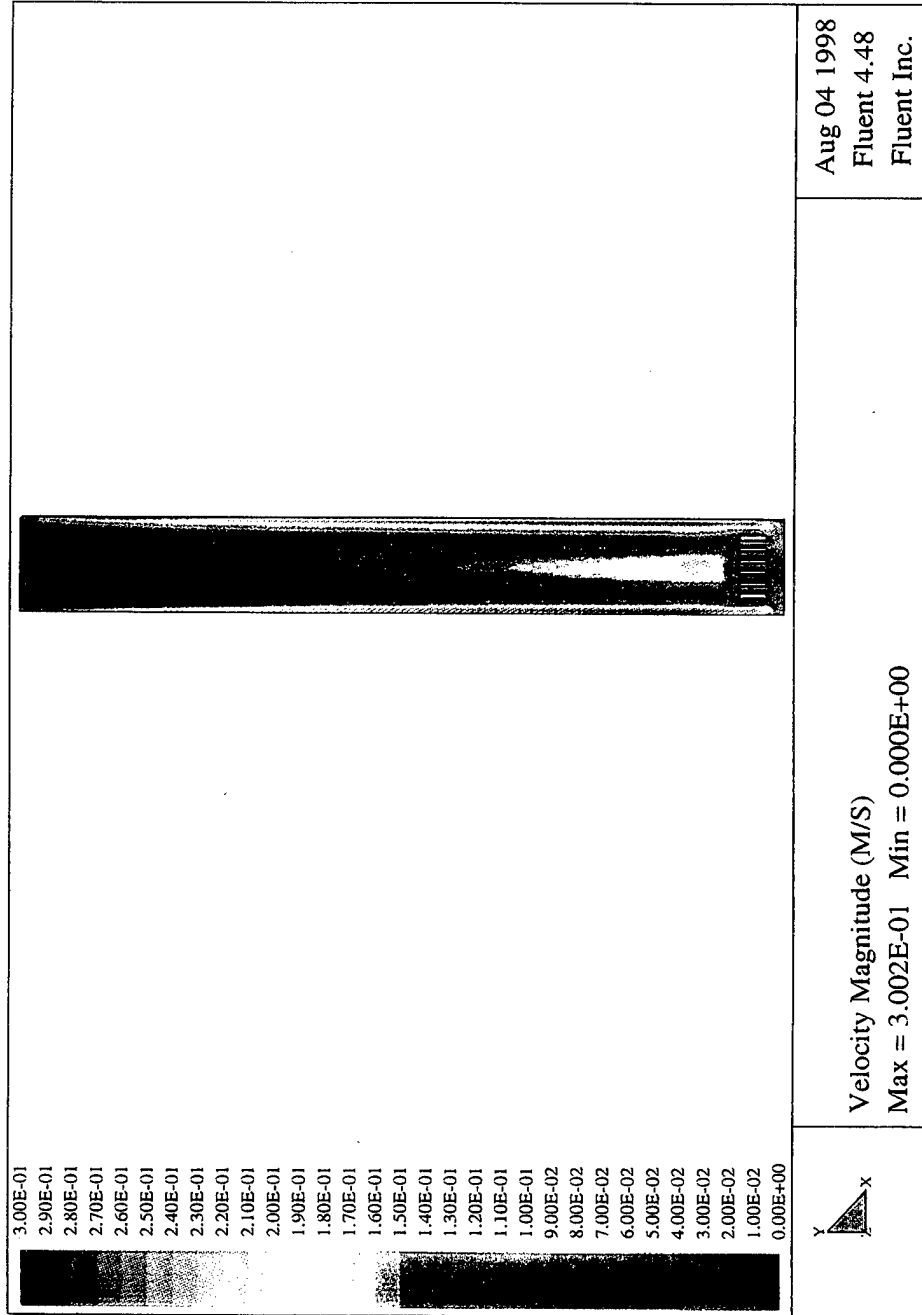
B.4: AR=4



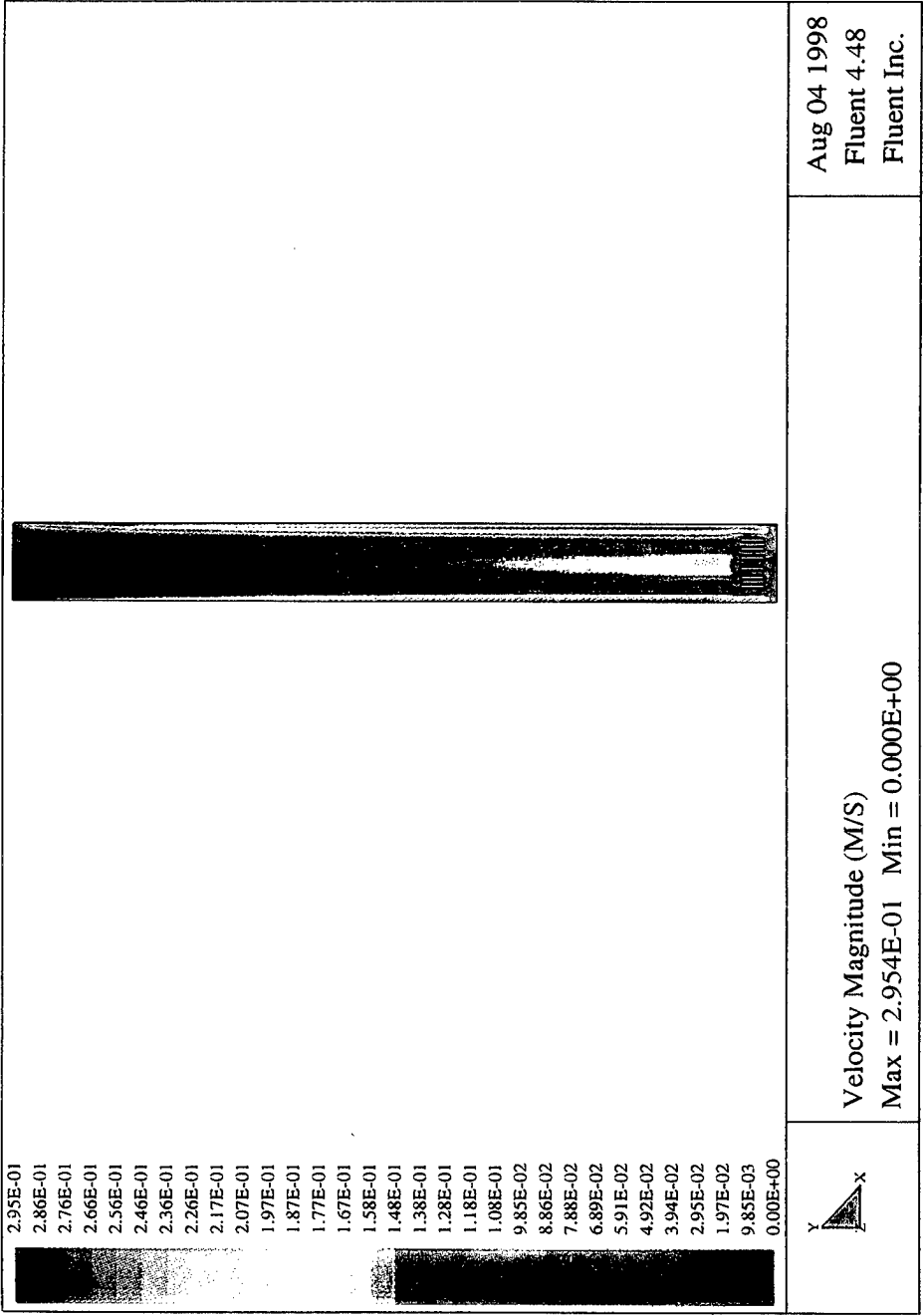
B.5: AR=6



B.6: AR=8



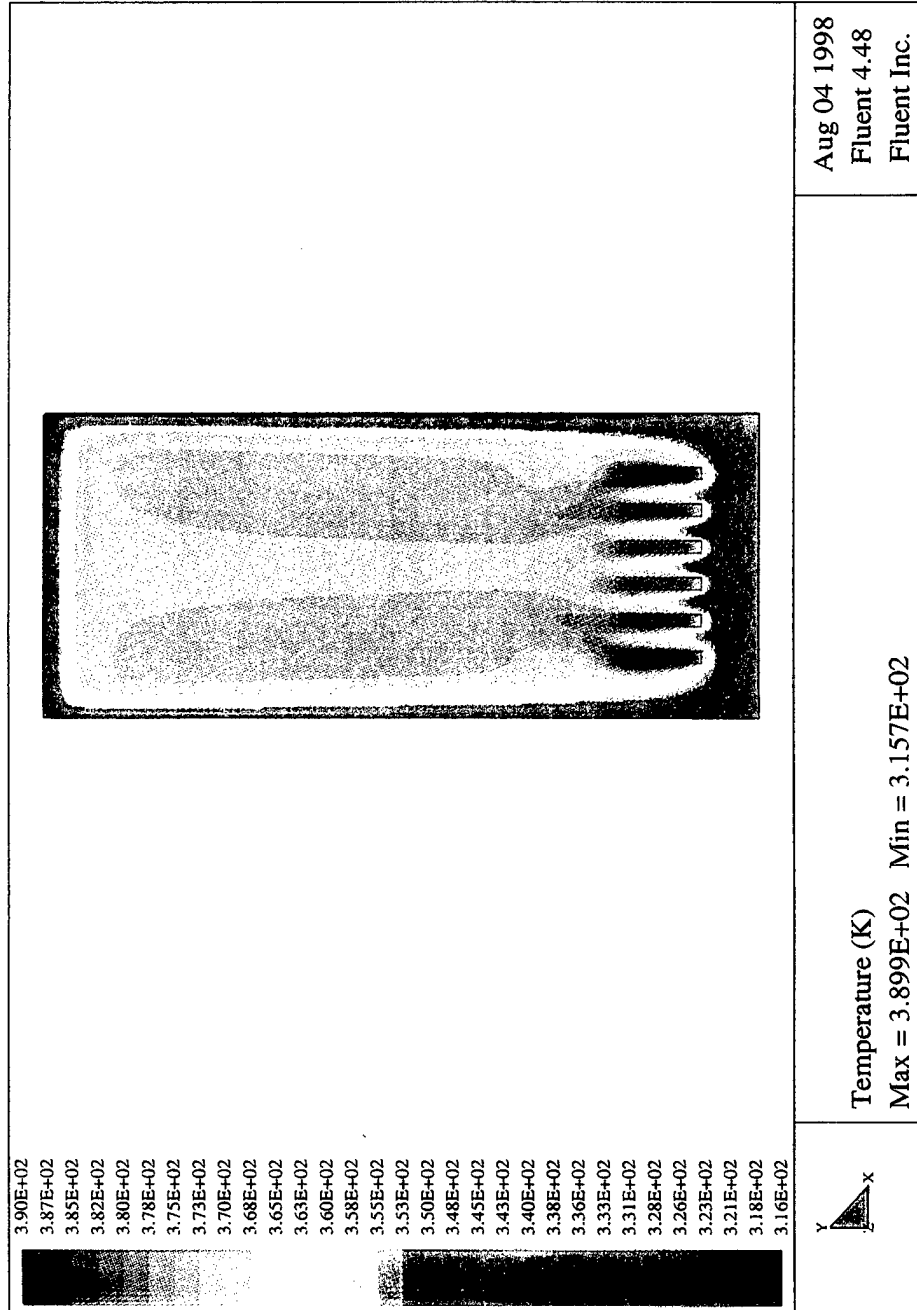
B.7: AR=10



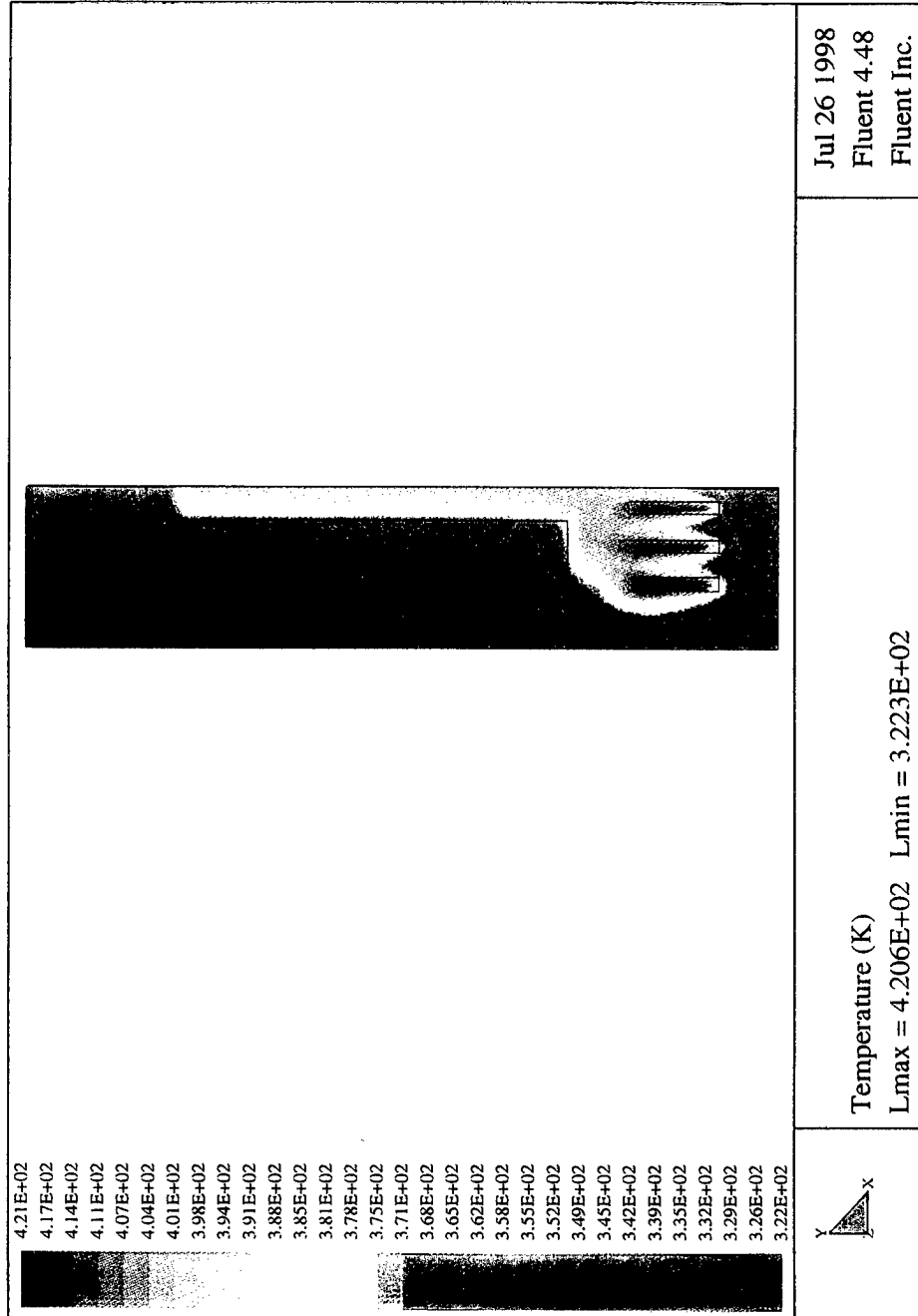
APPENDIX C:

TEMPERATURE CONTOUR PLOTS FOR $AR=2$

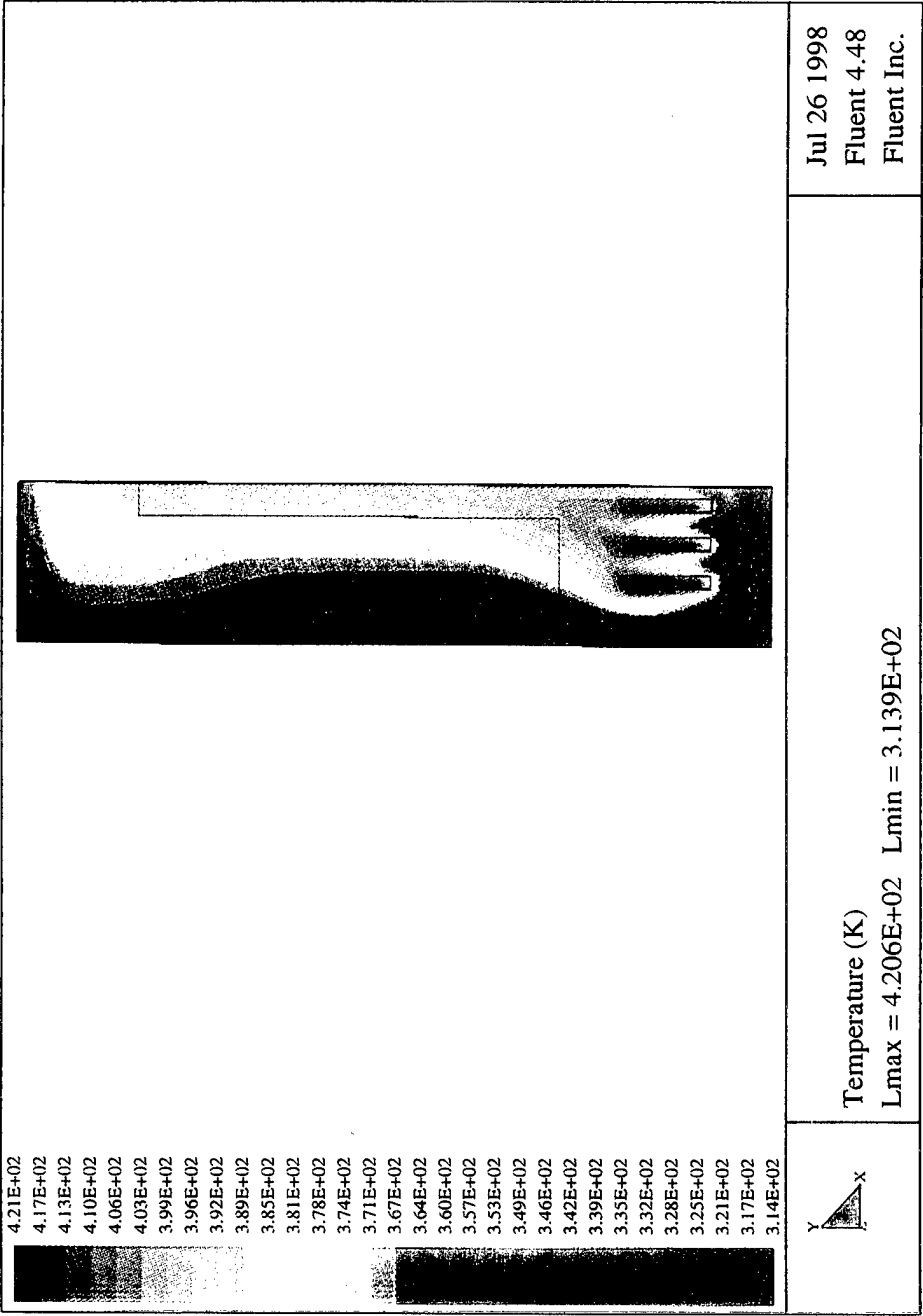
C.1: No Fins, Radiation



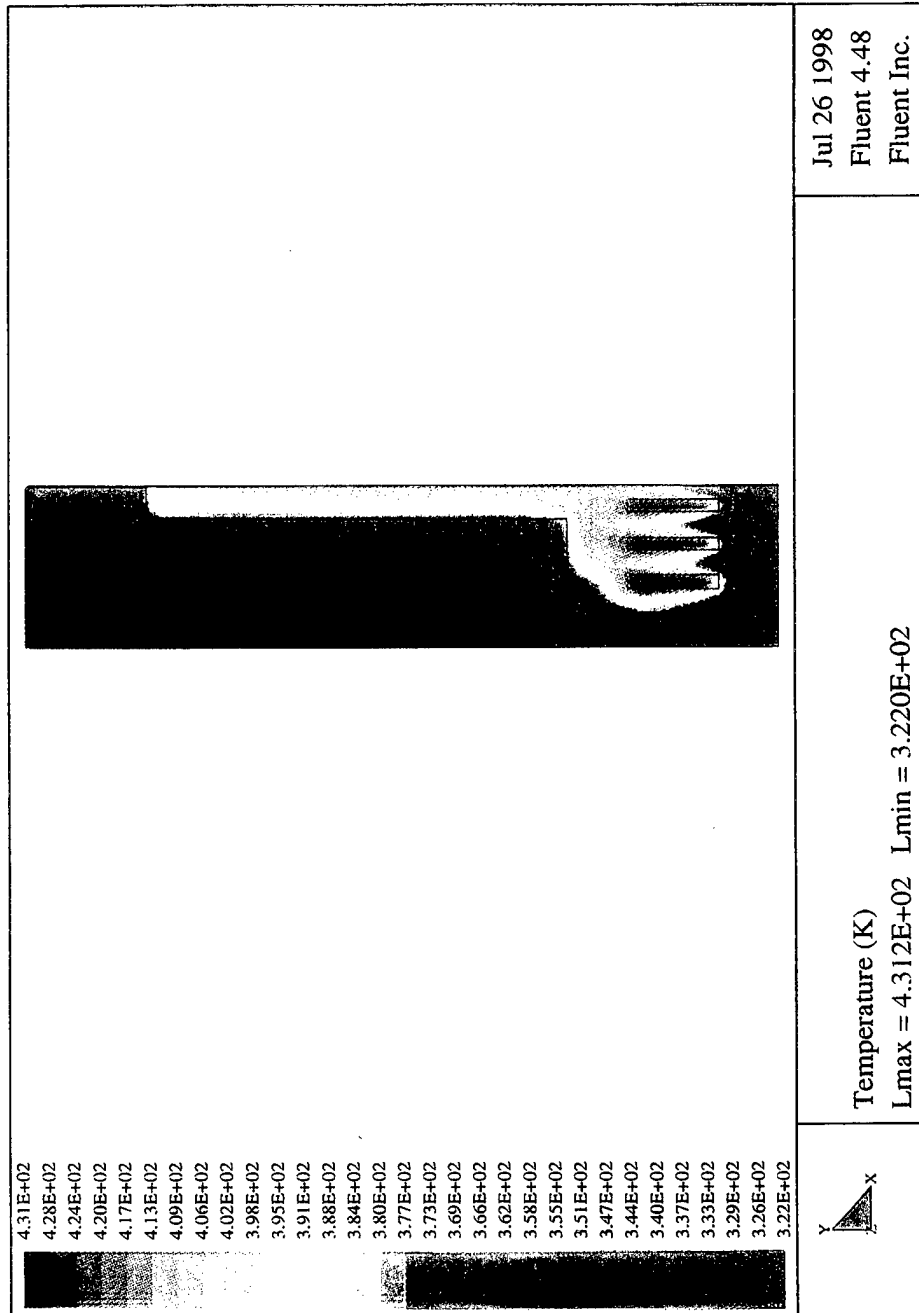
C.2: Fins, No Radiation (Near Fin)



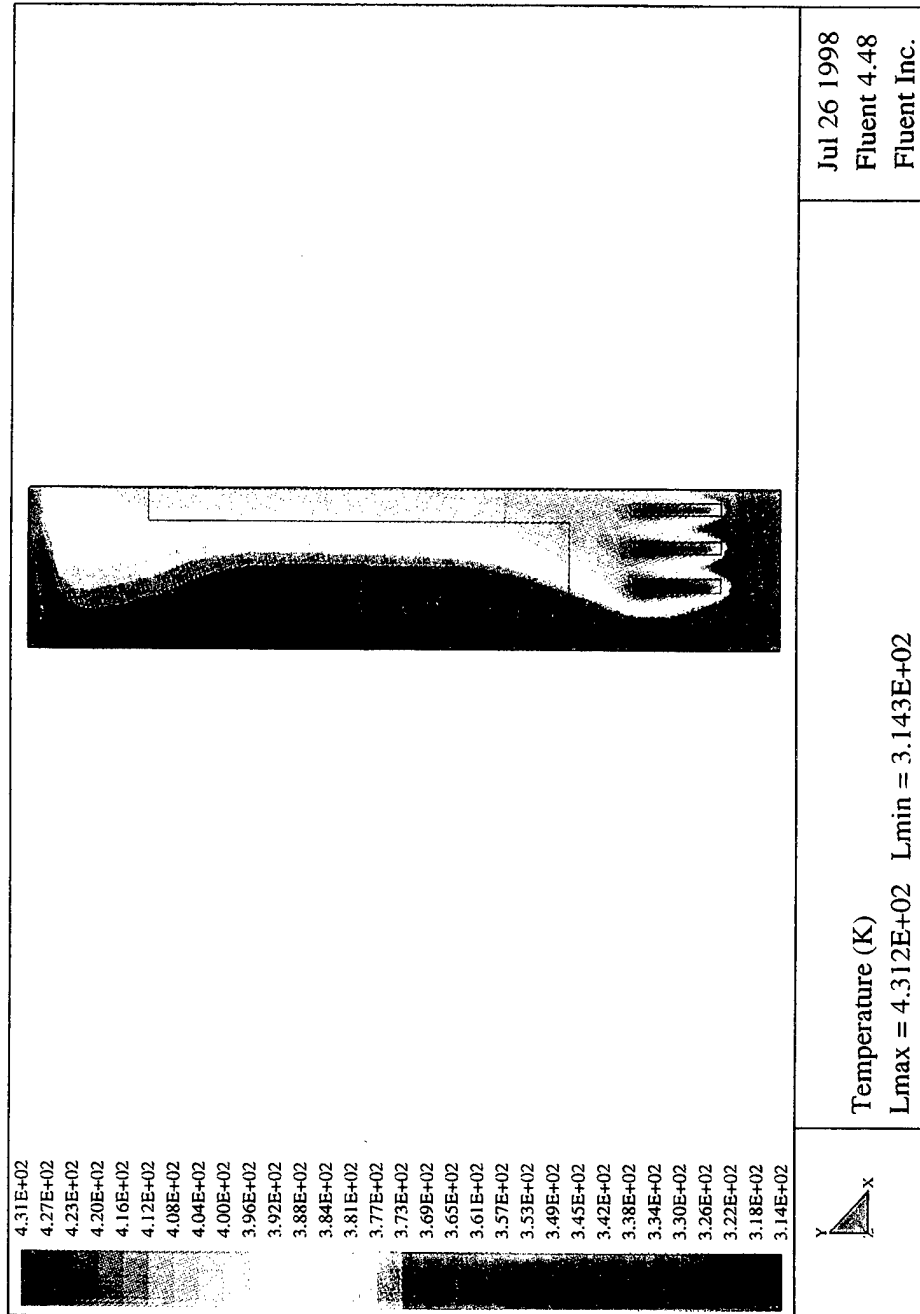
C.3: Fins, No Radiation (Between Fins)



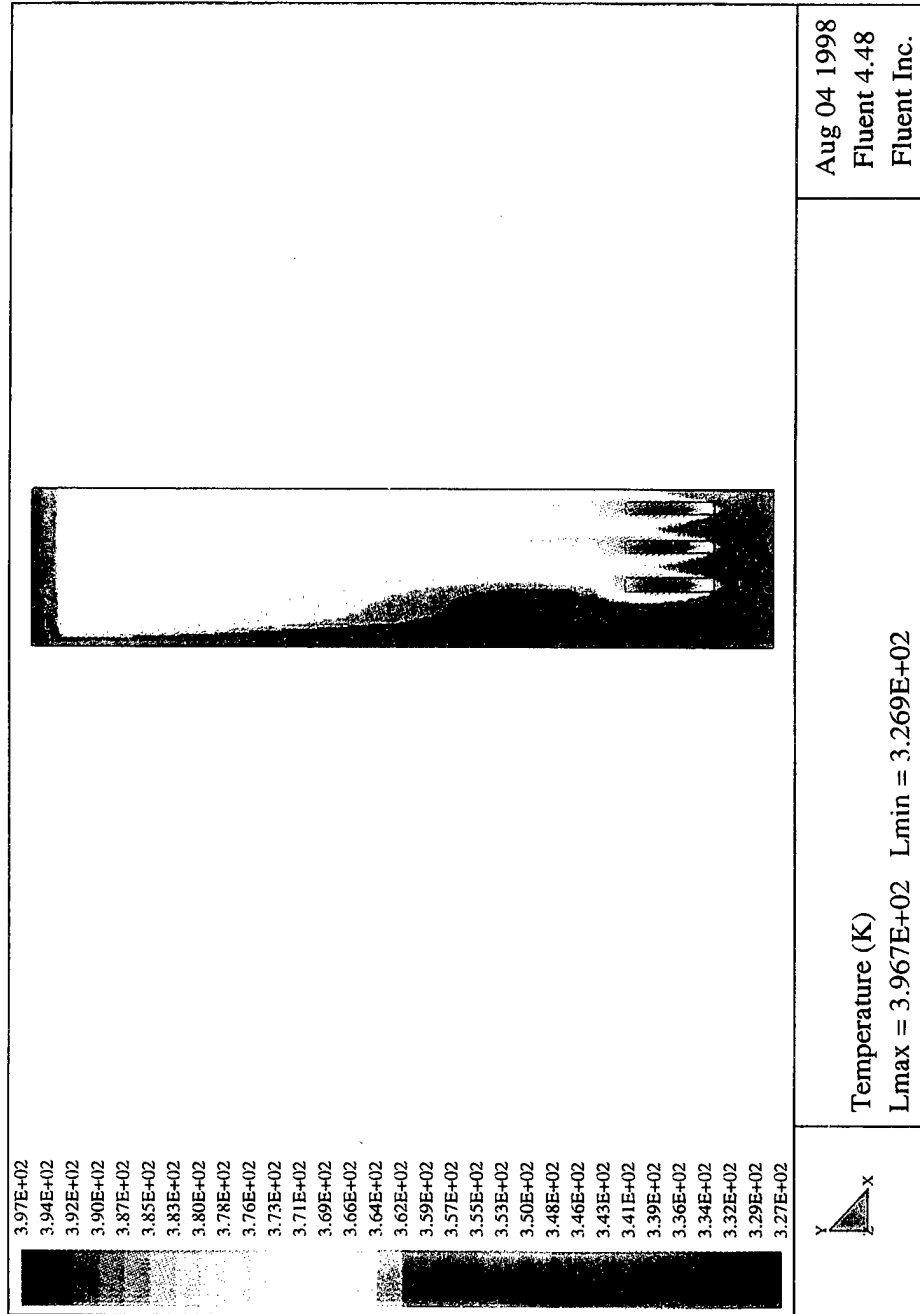
C.4: Fins & Radiation (Near Fin)



C.5: Fins & Radiation (Between Fins)

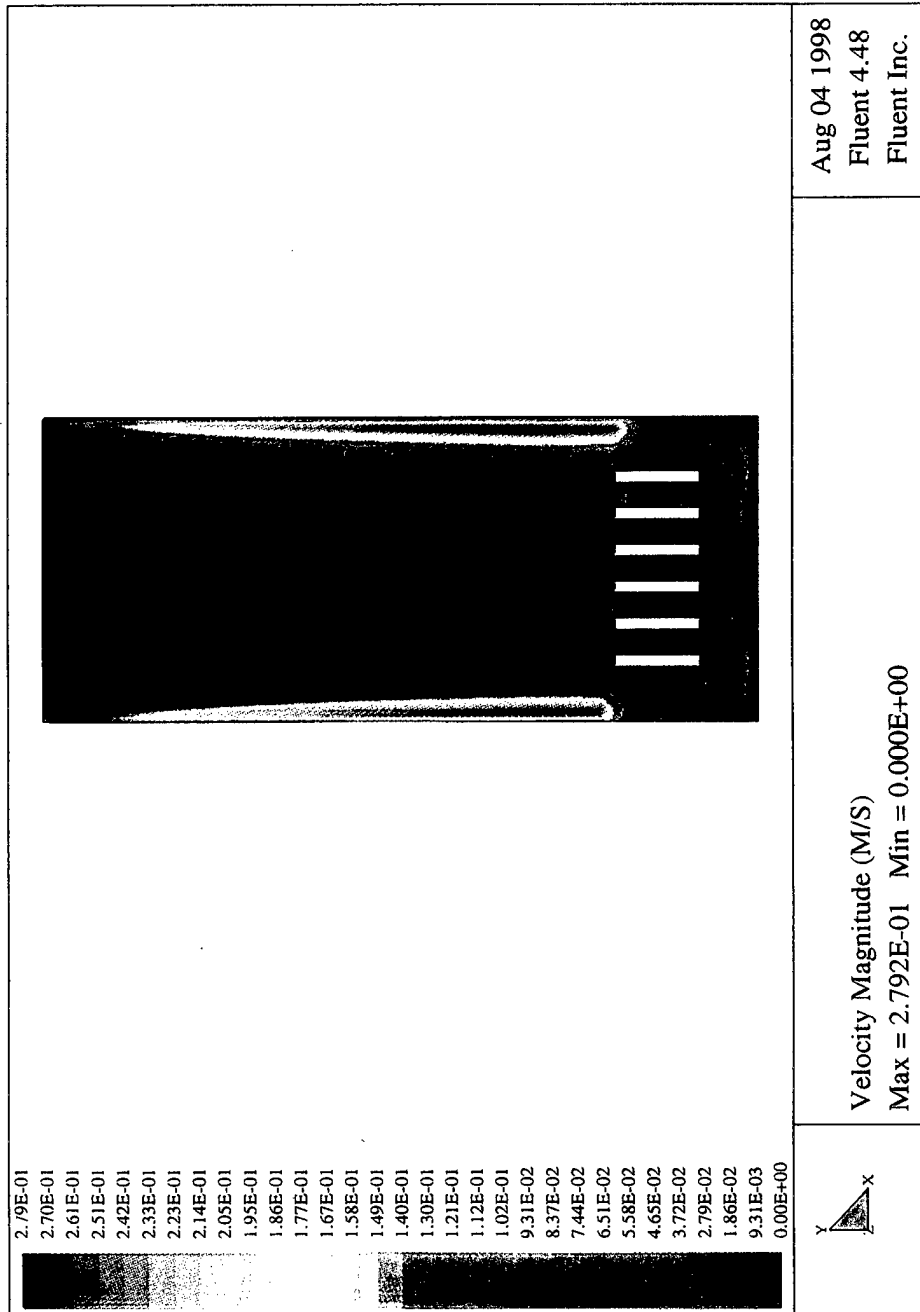


C.6: 3-D Plane Wall (At Centerline)

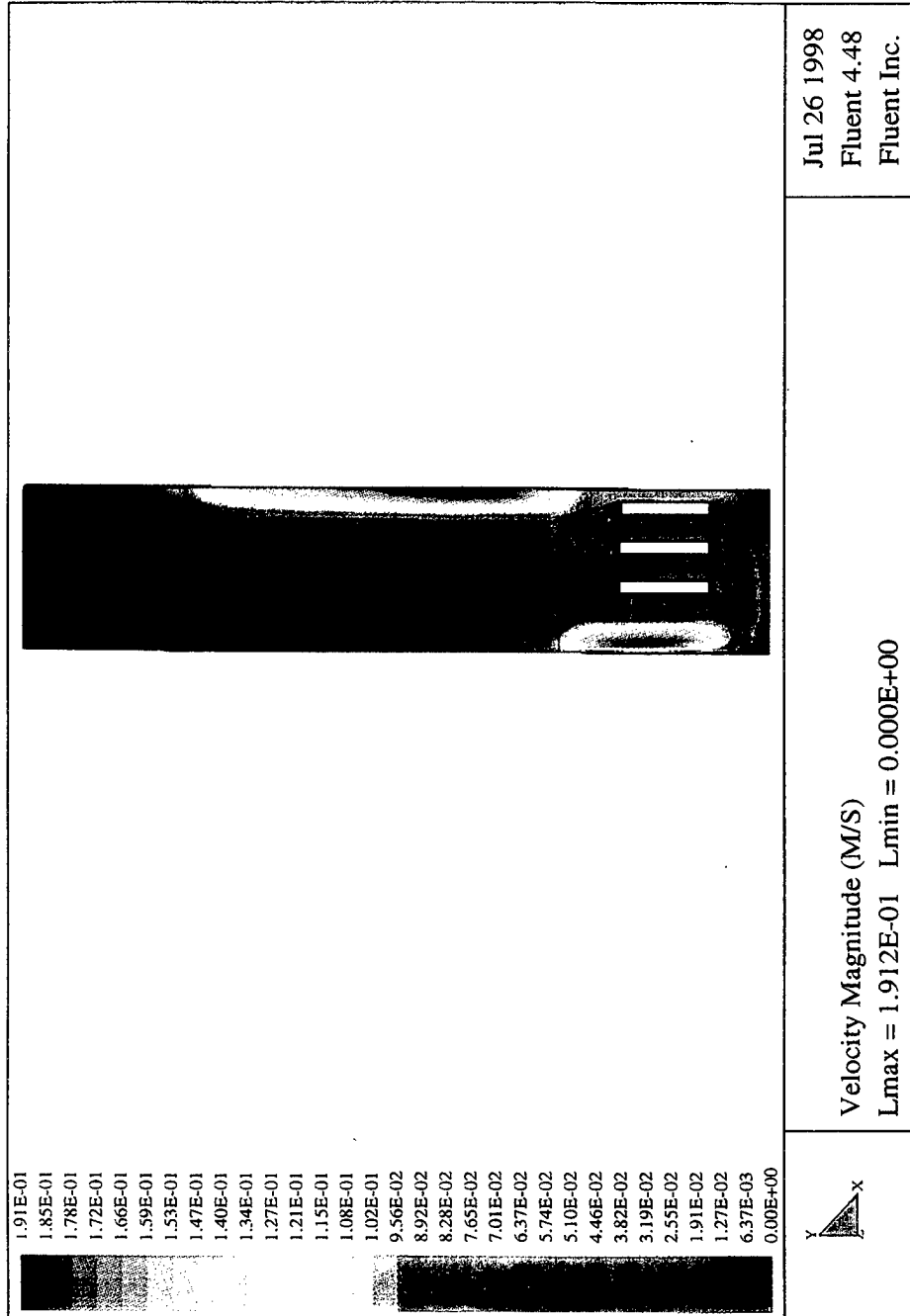


APPENDIX D:
VELOCITY CONTOUR PLOTS FOR $AR=2$

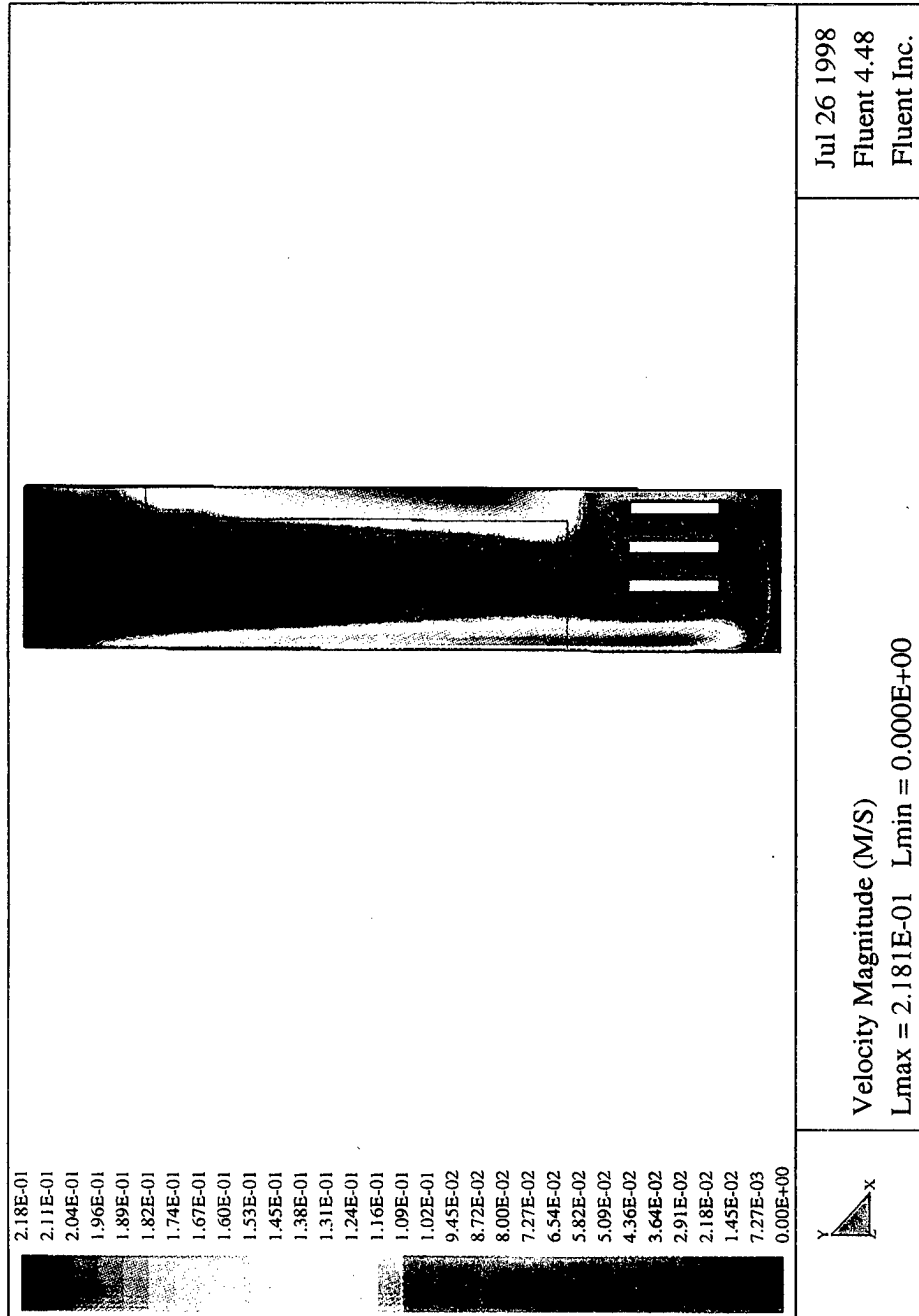
D.1: No Fins, Radiation



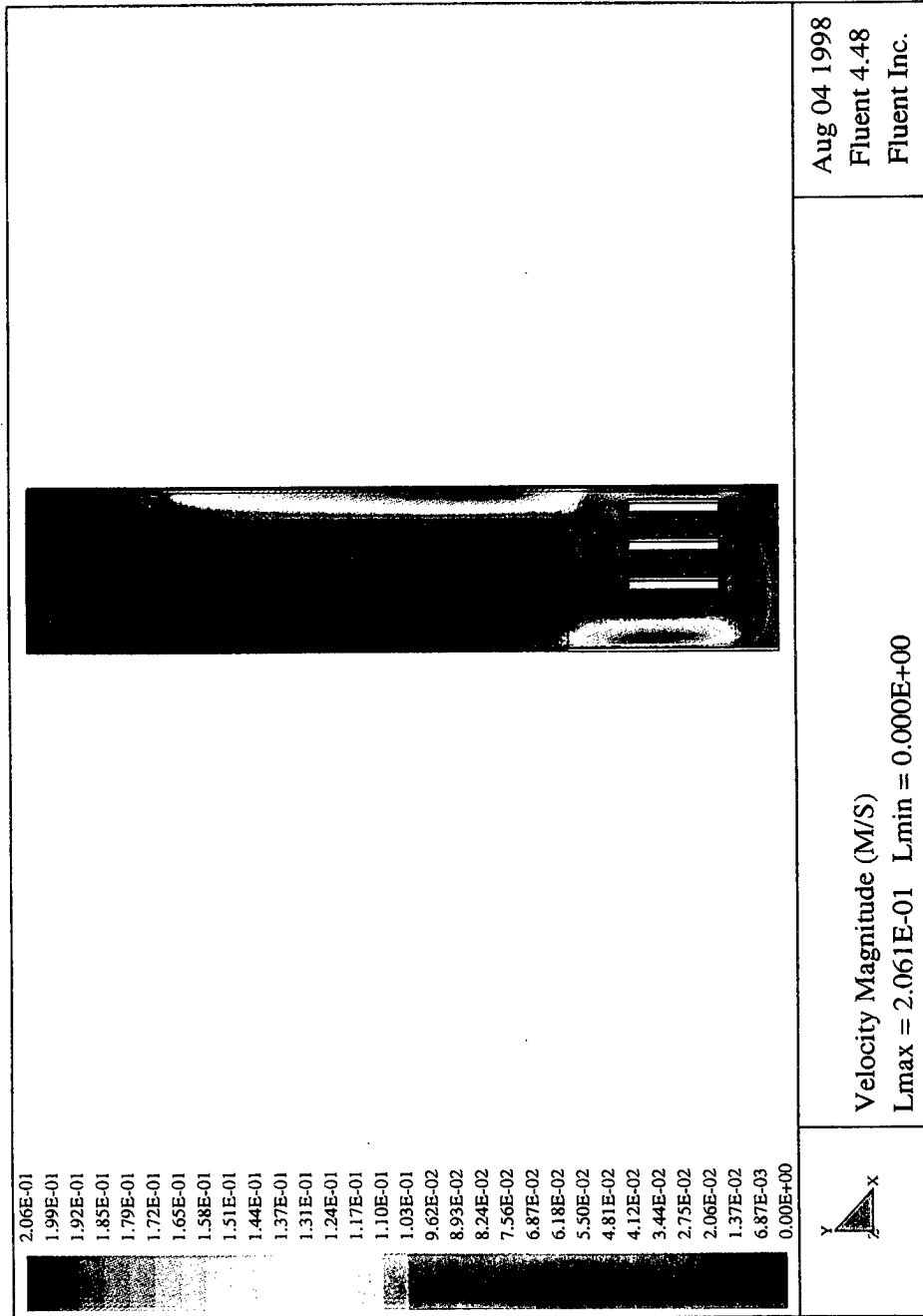
D.2: Fins, No Radiation (Near Fin)



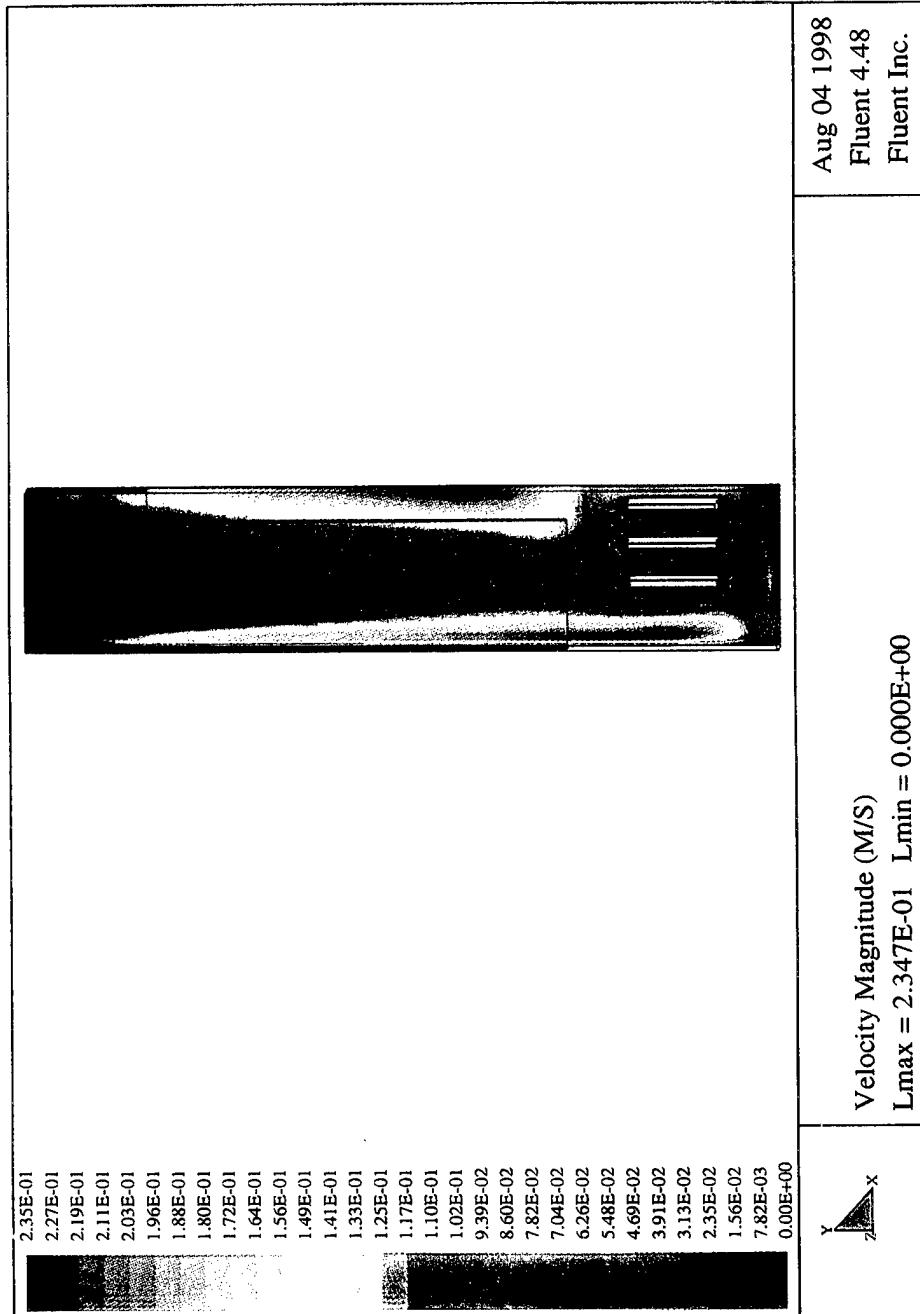
D.3: Fins, No Radiation (Between Fins)



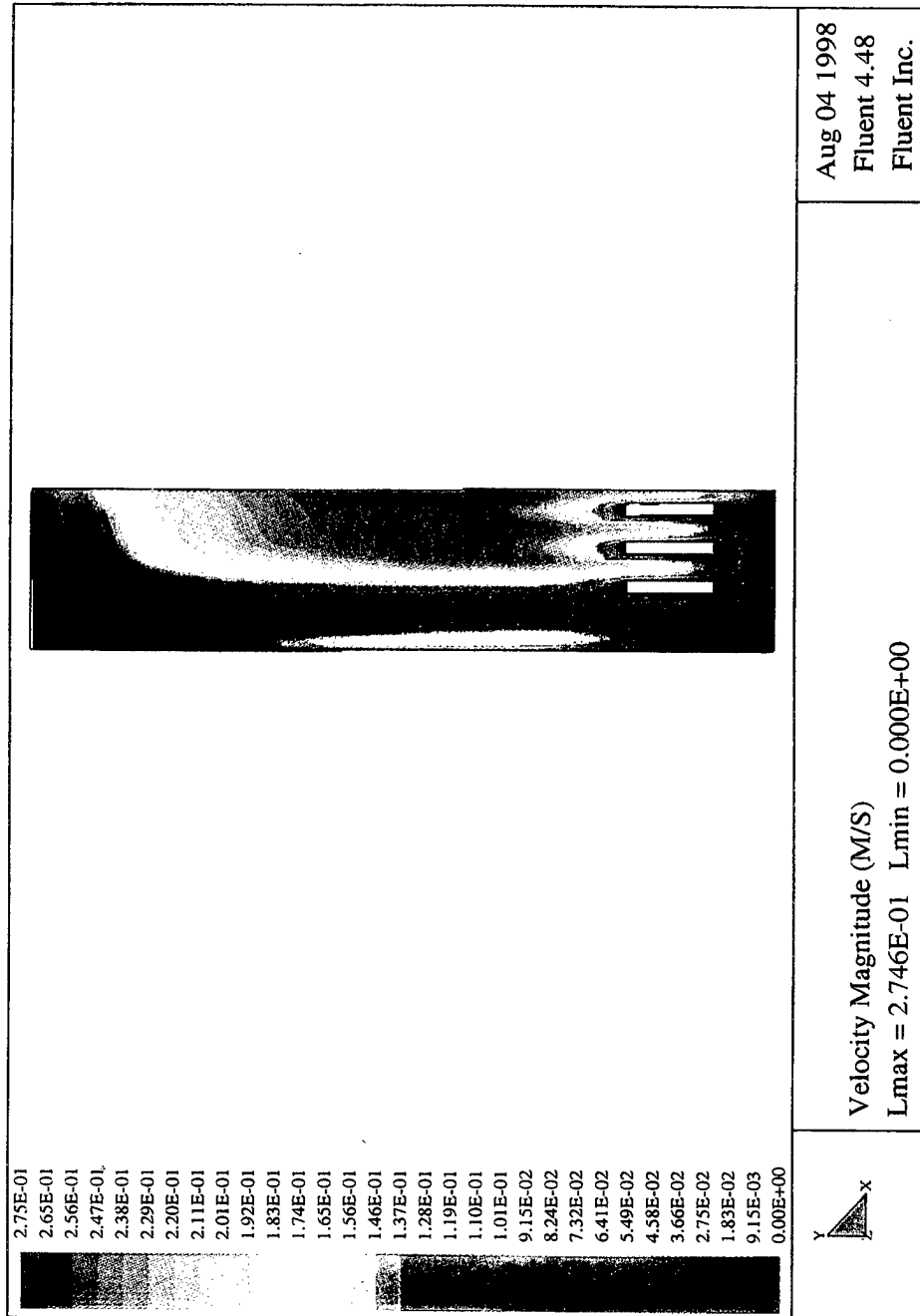
D.4: Fins & Radiation (Near Fin)



D.5: Fins & Radiation (Between Fins)



D.6: 3-D Plane Wall (At Centerline)



BIBLIOGRAPHY

Bar-Cohen, A. 1992, State-of-the-art in the Thermal Packaging of Electronic Equipment, J. of Electronic Packaging, vol. 114. pp. 257-270.

Chu, H.H., Churchill, S.W. & Patterson, C.V.S. 1976, The Effect of Heater Size, Location, Aspect Ratio and Boundary Conditions on Two-Dimensional, Laminar Natural Convection in Rectangular Channels, J. of Heat Transfer, vol. 98, pp. 194-201.

Eposito, P., and Behnia, M. 1994, Transition to Unsteadiness in Three-Dimensional Low Prandtl Natural Convection, Proc. 10th Int. Heat Transfer Conf., Brighton, vol. 7, pp. 43-48.

Ganzarolli, M., and Milanez, L. 1994, Influence of the Aspect Ratio on the Natural Convection on a Tall Cavity Heated from Below, Proc. 10th Int. Heat Transfer Conf., Brighton, vol. 7, pp. 55-60.

Hall, David. Telephone Interview. May 1998.

Johnson, G.E. 1986, Evolution of Correlations for Natural Convection Cooling of Electronic Equipment, ASME HTD vol. 57, pp. 103-111.

Karagiozis, A., Raithby, G. & Hollands, K. 1994, Natural Convection Heat Transfer from Arrays of Isothermal Triangular Fins in Air, J. of Heat Transfer, vol. 116, pp. 105-111.

Mills, A. F. Basic Heat and Mass Transfer. Chicago: Irwin, 1995.

Nakayama, W. & Bergles, A. E. 1990, Cooling Electronic Equipment: Past, Present, and Future, Heat Transfer in Electronics and Microelectronic Equipment, ed. Bergles A. E., pp. 3-39.

Poulikakos, D. 1985, Natural Convection in a Confined Fluid-Filled Space Driven by a Single Vertical Wall with Warm and Cold Regions, Journal of Heat Transfer, vol. 107, pp. 867-876.

Prasad, V., Keyhani, M. & Shen, R. 1990, Free Convection in a Discretely Heated Vertical Enclosure: Effect of Prandtl Number and Cavity Size, J. of Electronic Packaging, vol. 112, pp. 63-74.

Shen, R., Prasad, V. & Keyhani, M. 1989, Effect of Aspect Ratio and Size of Heat Source on Free Convection in a Discretely Heated Vertical Cavity, Numerical Simulation of Convection in Electronic Equipment Cooling, ASME HTD, vol. 121, pp. 45-54

Vliet, G.C. & C.K. Lui. An Experimental Study of Turbulent Natural Convection Boundary Layers. ASME Journal of Heat Transfer, Nov. 1969, pp. 517-531.

VITA

James Wilson Stahl was born in Houston, Texas on September 20, 1974, the son of John Wilson Stahl and Lana Sue Stahl. After completing his work at Pearland High School in Pearland, Texas in 1993, he received an appointment to the United States Air Force Academy, Colorado. In May 1997 he was commissioned as a second lieutenant in the United States Air Force, and received the degree of Bachelor of Science in Engineering from the United States Air Force Academy. He majored in mechanical engineering and also received a math minor. In August, 1997 he entered the Graduate School at the University of Texas at Austin and received the degree of Master of Science in Engineering in August 1998. He will be attending jet pilot training for the Air Force in September 1998.

Permanent Address: 1408 Briar Crest

Pearland, Tx 77581

The thesis was typed by the author.